INSIGHT

"ImplementatioN in real SOFC Systems of monItoring and diaGnostic tools using signal analysis to increase tHeir lifeTime"

Grant Agreement n° 735918 –
Research and Innovation Project

Deliverable D2.2. Failure analysis and critical lifetime parameters for SOFC system

Start date of the project: 1st January 2017
Duration: 36 months
Project Coordinator: Julie MOUGIN – CEA

Contact: Julie MOUGIN – CEA LITEN France - julie.mougin@cea.fr

Document Classification

Title	Failure analysis and critical lifetime parameters for SOFC system
Deliverable	D2.2
Reporting Period:	P1
Date of Delivery foreseen	M4 – April 2017
Draft delivery date	2017-Sep-25
Validation date	22/12/2017 for final approval

Authors	J Van herle
Work package	WP2 Experimental testing and Calibration
Dissemination	PU
Nature	R
Version	*V1*
Doc ID Code	D2_2_4_EPFL_20170925
Keywords	

Document Validation

Partner	Approval (Signature or e-mail reference)
P1 - CEA	e-mail
P2 - DTU	
P3 - UNISA	
P4 - EPFL	
P5 - JSI	
P6 - VTT	
P7 - AVL	
P8 –SP	
P9 - HTc	
P10 – BIT	
P11 – AK	

This project has received funding from the Fuel Cells and Hydrogen 2 Joint Undertaking under grant agreement No 735918. This Joint Undertaking receives support from the European Union's Horizon 2020 research and innovation programme and Hydrogen Europe and N.ERGHY

Document Abstract

A detailed review of SOFC degradation processes was carried out, with an update from the literature and a return of experience from field and stack testing by the partners. A compiled file was circulated to partners for assessment and priority ranking of the various processes. Account was taken of the severity and frequency of the degradation phenomena, their detectability, and potential for mitigation or recovery measures. With this approach, a final ranking was made which proposes 3 processes to investigate in detail in INSIGHT: anode reoxidation, carbon deposition and seal leakage.

Table of Contents

Abbreviations

/

1. Context and initial assessment

The aim of this task

Task 2.1 – Main faults and degradation phenomena. From M1 to M4
Task leader: P4 EPFL – Participants: CEA, DTU, SP, HTC, VTT

was to select the most important

· Faults to be detected;
· Degradation phenomena to be accounted for lifetime.

To achieve this goal, a review of the open literature was performed with focus on SOFC stack and system durability and **most critical degradation phenomena, including means to identify, avoid or counteract them**. A list of critical faults/failures is given and detailed with their causes, effects, detection and possible counter measures. Based on the previous experience in cell, SRU and stack testing, EPFL, CEA, DTU, SP, HTC and VTT contributed to the definition and description of the most important fault events and conditions leading to accelerated degradation during life time.

Apart from the bibliography, HTc also analysed **operational failure statistics** based on deployed systems in real operation in order to identify stack typical failure. Indeed, the identification of feasible counter actions is a key issue for a stack designer and manufacturer, therefore important efforts are developed to understand how to perform them without increasing the costs.

A table was compiled enumerating all known degradation phenomena and circulated to the partners for completion. Based on this input, the info and preferences below emerged for the partner literature review, the partner contribution to the Deliverable, and the phenomena to focus on in INSIGHT, with their detection potential and mitigation potential. Phenomena were selected based on **severity, detection potential and recovery potential** (fully, partially, or at least a potential of stopping or reducing further degradation). A provisional list from the time of the INSIGHT proposal writing suggested the following potential priority phenomena: a) **Fuel starvation**, b) **Gas leakage**, c) **C/S poisoning.**

Table 1: Initial subtask distribution (literature overview) and assessment of the main stack components

Component	Partner	Degradation cause	Detection	Recovery/ Mitigation potential
Anode	DTU	Sulfur poisoning	rapid small voltage drop; low cost sulfur-detector at outlet (in case of breakthrough); the reformer will get poisoned first, before the stack=> possibly detected by reformer temperature deviation	reversible (for concentration < 100 ppm and short exposure) when contaminant stream stops
		Carbon deposition	increase in ΔP across stack anode; too low O/C ratio; if reformer gets damaged by carbon deposition before the stack: reformer temperature deviation	Steam / CO_2 flush
		Ni coarsening	R_{ct} response at 1-2 kHz	partial recovery by current treatment
		Contaminants in general	R_{ct} response at 1-2 kHz; Contaminant- specific detector	need for redox cells in order to flush the anodes from contaminants; else a system-protected reoxidation, e.g. a flush at 500°C, sufficiently low T to not destroy the Ni anode
Sealing materials, sealing techniques	VTT	Cracks, porosity, volatility, materials reaction	OCV loss humidity in cathode outlet	recuring at increased temperature; minimize Δp across cells, stacks
Cathode	CEA	Cr poisoning	R_{ct} of cathode	revolatilize deposited Cr by operation at OCV or SOEC condition
		$SrCrO_4$ formation	R_{ct} of cathode + increase in R_Ω; shift of Nyquist plot, increase in 3rd arc	minimize cathode side humidity
MIC	EPFL	Contact loss with GDL (CCCL/ACCL)	increase in R_Ω	temperature excursion with/without increased compression
		Channel blocking or deformation	ΔP; EIS gas conversion response EIS diffusion response	likely none
		Scale formation	increase in R-ohmic; (ΔP cathode – very small variation)	minimize cathode side humidity
Electrolytes YSZ/CGO	HTc, EPFL	Cracks, leakage	OCV loss Temperature increase EIS?	likely none

Operational experience

Feedback from SP/HTc on statistical failure analysis from field tests and operational experience gave the following main occurrences and observations:

a) Stack mechanical failure (leaks, contact loss,…)
=> any recovery is difficult and the main measures are milder operating conditions; eventually the stack has to be replaced.

b) Various BoP issues:
   - gas / water / air supply
   - fuel processing
   - burner
   - offgas control
   - heat recovery
   - control and safety hardware / software
   - power electronics
   - instrumentation

From the stack producer and system operators' point of view, there is a **need for**:

- more detailed stack monitoring; e.g. sensing by **THDA** on the stack electrical output (voltage, current)
- monitoring of the quality & amount of gas (reformate, air) that arrives at the stack, and of the stack temperature, in particular sudden temperature changes

In terms of poisoning phenomena,
- Cr poses no more real issue;
- S remains an issue at the anode; but recovery seems possible when poisoning is mild (low ppm, short exposure)
- S (from SO_2 polluted air) is equally a concern at the cathode (=>formation of $SrSO_4$); the potential for recovery could be explored by reverse polarization.

A general comment and observation (made by VTT) is that reverse polarization, either as electrolysis treatment or as current treatment in electrolysis mode without H_2O supply, might recover SOFC performance in several ways and that this is a potential recovery strategy to be explored.

Finally, some phenomena are of relatively less interest, mainly because they are known to be irreversible:
- MIC corrosion
- delamination
- compression loss

2. Considered degradation processes and risk assessment

In the following, damaging phenomena are classified through the definition of risk, i.e. the severity of the process multiplied with the occurrence probability of the process. A priority classification is arbitrarily proposed as: severity class 3,2,1; and occurrence class 3,2,1. This then leads to the following possible combinations for classification:

Severity	Occurrence	Risk
3	3	9
3	2	6
2	3	6
2	2	4
3	1	3
1	3	3
1	2	2
2	1	2
1	1	1

Based on the partner survey, the considered processes were organized as follows:

Table 2 : Classification of degradation processes

Components	Processes
Anode	An1. Ni coarsening
	An2. Ni reoxidation
	An3. C deposition
	An4. S poisoning (+ other poisoning)
Cathode	Cath1. 2nd phase formation ($SrZrO_3$)
	Cath2. Decomposition (Sr mobility/activity)
MIC	MIC1. Contact loss (spallation, delamination, deformation, creep)
	MIC2. Corrosion: Cr-scale (=>poisoning), Si-scale, Fe-diffusion
Seals	Seal1. Mechanical failure (leakage)
	Seal2. Decomposition, reactivity, volatility (=>poisoning)
Electrolytes	Ely1. Cracks, embrittlement, CGO porosity
	Ely2. Conductivity loss, YSZ-CGO reactivity

3. Detection

The detectability of responses, based on the EIS frequency regime in which they occur, according to present knowledge, is given by:

Table 3 : Detectable SOFC EIS responses according to frequency regime and potential relation to degradation processes:

Response	Attribution	Frequency peak	Influenced by	Related to (Table 2)
P1	probably O_2 dissociation	< 1 Hz	j, T	Cath2, (Cath1), (MIC2), (Seal2)
P2	gas conversion	few Hz	j, T, pH_2O, dilution	An1, An2, An3, (An4), Seal1, Ely1
P3	cathode R_{pol}	10-100 Hz	j, T, pO_2	Cath2, (Cath1), (MIC2), (Seal2)
P4	likely anode diffusion	100-500 Hz	j, T, pH_2O, dilution	An1, An2, An3, (An4), Seal1, Ely1
P5	anode R_{pol} (ct)	1-4 kHz	j, T, pH_2O, dilution	An1, An2, An3, An4, (Seal2)
P6	ion transfer at cathode side	> 5 kHz	T, pO_2	(Cath1), Cath2, Ely1, Ely2
R_Ω	anything ohmic	intercept (corrected)	T	MIC1, MIC2 Ely1, Ely2 An1, An2, An3, (An4) Cath1, (Cath2)

We see that there are hardly unique correlations.

4. Anode literature review study

4.1 Sulfur poisoning (Process : An4)

Causes

Available experimental studies mainly focus on H_2/H_2O based systems containing H_2S (Rasmussen & Hagen, 2009; Matsuzaki & Yasuda, 2000; Cheng & Liu, 2007; Sasaki, et al., 2006; Yang, Cheng, Liu, & Wilson, 2010), however newer studies are dedicated to investigate the effect in application oriented hydrocarbon-containing fuel mixtures (Rasmussen & Hagen, 2010; Smith, Wood, & Birss, 2009; Yoshizumi, Taniguchi, Shiratori, & Sasaki, 2012; Weber, Dierickx, Kromp, & Ivers-Tiffee, 2013; Li, et al., 2014; Hagen, Sulfur Poisoning of the Water Gas Shift Reaction on Anode Supported Solid Oxide Fuel Cells, 2013; Shiratori, Ijichi, Oshima, & Sasaki, 2010; Papurello, et al., 2016). In any of the investigated cases, a fast performance decay can be observed, which in some cases is followed by an additional long-term degradation process (Sasaki, et al., 2006; Yang, Cheng, Liu, & Wilson, 2010; Zha, Cheng, & Liu, 2007).
The initial voltage drop is associated to the blockage of TPBs by adsorbed sulphur. A general agreement regarding severity of the performance loss with respect to temperature (Matsuzaki & Yasuda, 2000; Sasaki, et al., 2006; Zha, Cheng, & Liu, 2007) and concentration of sulphur species (Rasmussen & Hagen, 2009; Matsuzaki & Yasuda, 2000; Cheng & Liu, 2007; Sasaki, et al., 2006; Yang, Cheng, Liu, & Wilson, 2010) exists. Lowering temperature and increasing sulphur concentration tend to enhance the phenomena as a result of higher sulphur coverage. Yet, the impact of current density is still controversial as current density has a rather complex effect on the (electro-) catalytic processes involved. (Sasaki, et al., 2006; Lohsoontorn, Brett, & Brandon, 2008; Zha, Cheng, & Liu, 2007; Hauch, Hagen, Hjelm, & Ramos, 2014; Ivey, Brightman, & Brandon, 2010; Kishimoto, et al., 2010; Brightman, Ivey, Brett, & Brandon, 2011; Hagen, Johnson, & Hjalmarsson, Electrochemical evaluation of sulfur poisoning in a methane-fuelled solid oxide fuel cell: Effect of current density and sulfur concentration, 2014).

In hydrocarbon based fuels the poisoning effect of sulphur is generally larger. Already at OCV conditions an effect of sulphur can be observed (Smith, Wood, & Birss, 2009; Rasmussen & Hagen, 2010; Hagen, Johnson, & Hjalmarsson, Electrochemical evaluation of sulfur poisoning in a methane-fuelled solid oxide fuel cell: Effect of current density and sulfur concentration, 2014; Hagen, Rasmussen, & Thydén, Durability of solid oxide fuel cells using sulfur containing fuels, 2011; Noponen, Halinen, Kiviaho, & Saarinen, 2006; Rostrup-Nielsen, Hansen, Helveg, Christiansen, & Jannasch, 2006). H_2S tends to severely alter the kinetics of the methane reforming and water-gas shift reaction. This impact seems to be even stronger than the impact on the electrochemical oxidation of hydrogen.

Long-term poisoning effects are less studied. Proposed explanations include (i) the formation of NiS_3 at high H_2S concentration (Dong, Cheng, Zha, & Liu, 2006), (ii) enhancement of Ni agglomeration due to dissolving sulphur in the Ni bulk structure (Zha, Cheng, & Liu, 2007; Kishimoto, et al., 2010) (iii) change of Ni particle shapes and Ni-diffusion away from the anode/electrolyte interface and so causing loss of percolation (Hauch, Hagen, Hjelm, & Ramos, 2014; Hagen, Rasmussen, & Thydén, Durability of solid oxide fuel cells using sulfur containing fuels, 2011).

Detection

Similar to degradation caused by Ni coarsening, no specific detection tool for sulfur poisoning or other impurities has been reported. Most likely, in EIS it would show up as P5 being affected (increased). Alternatively, S might be detected by sampling of the fuel feed gas line and sending it through a S-specific detecting material like Dräger tubes; the best location for this would be after the S-trap (to indicate saturation or breakthrough of the trap).

Recovery

If the exposure time is short enough (> few days) and the contaminant concentration low enough (a few ppm), the degradation is reversible, i.e. the anode slowly recovers when the contaminant stream stops. Alternatively, in the case of redox stable anodes, a redox cycle would remove the contaminant and regererate the anode. On the contrary, with high concentration and long exposure times, the anode is irreversibly damaged in its structure and chemistry (see above).

4.2 Carbon deposition (Process : An3)

Causes

Several experimental studies in simulated synthesis gas (Drewery, Kennedy, Alenazey, Dlugogorski, & Stockenhuber, 2015; Miao, et al., 2015; Zhang, Yang, & Wang, 2015; Chen, Wang, Miao, Li, & Xu, 2011; Alzate-Restrepo & Hill, 2010) or methane (Fan, Zhang, Hua, & Li, 2016; Jiao, et al., 2016; Millichamp, et al., 2013; Macek, Novosel, & Marincek, 2007; He & Hill, 2007; Triantafyllopoulos & Neophytides, 2003; Koh, Yoo, Park, & Lim, 2002; Takeguchi, et al., 2002; Lanzini, et al., 2016; Lanzini, et al., 2013) perform thermodynamic analysis in order to identify the regions where carbon formation is favourable. However, as it was shown by Sasaki et al. (Sasaki & Teraoka, Equilibria in Fuel Cell Gases: II. The C-H-O Ternary Diagrams, 2003) solid carbon can be formed even in the region where it was not predicted by equilibrium calculations.
A recent study by Kuhn and Kessler (Kuhn & Kesler, Carbon deposition thresholds on nickel-based solid oxide fuel cell anodes I. Fuel utilization, 2015; Kuhn & Kesler, Carbon deposition thresholds on nickel-based solid oxide fuel cell anodes II. Steam:carbon ratio and current density, 2015) investigated threshold for different operating parameters i.e. FU, S/C ratio, current density and temperature. Their thermodynamic threshold calculations were based on the assumption that carbon is deposited as solid graphite. They concluded that above 700oC thermodynamic data can be used to predict thresholds, while thresholds below 600oC strongly disagree. Similarly, He et al. (He & Hill, 2007) and Lee et al. (Lee, Hanna, & Ghoniem, 2013) came to the conclusion that thermodynamic, physical and kinetic properties of graphite cannot solely explain the details for anode degradation. Different forms of deposited carbon are reported ranging from nanotubes and fibers to dissolved carbon (He & Hill, 2007) and furthermore whisker-type structures (Lanzini, et al., 2013). Yet, the major aspects determining coking are certainly (i) temperature (Chen, Wang, Miao, Li, & Xu, 2011) and (ii) polarization (Lin, Zhan, Liu, & Barnett, 2005; Lin, Zhan, & Barnett, Improving the stability of direct-methane solid oxide fuel cells using anode barrier layers, 2006; Liu & Barnett, 2003). A recent literature overview can be found under (Khan, et al., 2016).

Detection

Recently, a methodology based on the EIS method was proposed by Subotic et al. (Subotic, et al., 2016) to detect coking at a sufficient early stage. The method would allow counteracting before the problem occurs.
Other in-situ detection strategies are combining EIS and additional detection technique such as a novel microbalance sensor (Millichamp, et al., 2013) or evolving gas analysis (EGA) sensor (Kuhn & Kesler, Method for in situ carbon deposition measurement for solid oxide fuel cells, 2014). Although these studies allow in-situ detection, they only can detect deposition after it occurred.
Furthermore Raman Spectroscopy can be used (Blinn, et al., 2012).

Recovery

Concerning the recovery approach due to flushing, recent studies by Subotic et al investigate the recovery approach due to steam (Subotic, et al., 2015) and carbon dioxide flushing (Subotic, et al., 2016) in an auxiliary power unit (APU) unit operated with diesel reformate.
Gasification rates via H_2, CO_2 and steam treatment at 550°C were modelled and experimentally studied by Snoeck et al. (Snoeck, Froment, & Fowles, 2002). Depending on the carbon deposit – either formed by Boudouard reaction or methane cracking – different gasification processes are reported.
The recovery approach by CO_2 gasification of Ni-based catalysts was furthermore studied by Takenaka et al. (Takenaka, Kato, Tomikubo, & Otsuka, 2003; Takenaka, Shimizu, & Otsuka, Complete removal of carbon monoxide in hydrogen-rich gas stream through methanation over supported metal catalysts, 2004; Takenaka, Tomikubo, Kato, & Otsuka, 2004).

4.3 Ni coarsening (Process: An1)

Causes

The mobility of Ni-atoms can be influenced by operating parameters, i.e. mainly temperature (Hagen, Barfod, Hendriksen, Liu, & Ramousse, 2006; Thydén, 2008; Ananyev, et al., 2015), humidity of the fuel gas (Hauch, Mogensen, & Hagen, Ni/YSZ electrode degradation studied by impedance spectroscopy - Effect of p(H2O), 2011; Holzer, et al., 2011; Ploner, Hagen, & Hauch, In Press) and reduction and process parameters, thereby changing the initial microstructure (Jørgensen, Ebbehøj, & Hauch, 2015; Manukyan, et al., 2015; Jiao & Shikazono, 2015; Hauch, Jørgensen, Brodersen, & Mogensen, 2011). These effects result in lowering of the overall electrode performance by active surface area changes.

Detection

To the best of our knowledge, no in-situ detection tool specifically concerning Ni-coarsening has been reported. Only EIS measurement and analysis of the Ni-charge transfer reaction resistance may be used. (Hauch, Mogensen, & Hagen, Ni/YSZ electrode degradation studied by impedance spectroscopy - Effect of p(H2O), 2011)

Recovery

Reversed current treatment (RCT) (Klotz, et al., 2011; Szász, et al., 2017) might allow partial recovery of the coarsened Ni/YSZ microstructure due to the formation of a nanostructured anode functional layer interface.

4.4 Anode Bibliography

Alzate-Restrepo, V., & Hill, J. M. (2010). Carbon deposition on Ni/YSZ anodes exposed to CO/H2 feeds. *Journal of Power Sources, 195*(5), 1344-1351. Retrieved from http://www.sciencedirect.com/science/article/pii/S0378775309015535

Ananyev, M., Bronin, D., Osinkin, D., Eremin, V., Steinberger-Wilckens, R., de Haart, L., & Mertens, J. (2015). Characterization of Ni-cermet degradation phenomena I. Long term resistivity monitoring, image processing and X-ray fluorescence analysis. *J. Power Sources, 286*, 414-426. Retrieved from http://www.sciencedirect.com/science/article/pii/S0378775315006023

Blinn, K. S., Abernathy, H., Li, X., Liu, M., Bottomley, L. A., & Liu, M. (2012). Raman spectroscopic monitoring of carbon deposition on hydrocarbon-fed solid oxide fuel cell anodes. *Energy Environ. Sci., 5*(7), 7913-7917. Retrieved from http://dx.doi.org/10.1039/C2EE21499G

Brightman, E., Ivey, D., Brett, D., & Brandon, N. (2011). The effect of current density on H2S-poisoning of nickel-based solid oxide fuel cell anodes. *Journal of Power Sources, 196*(17), 7182-7187. Retrieved from http://www.sciencedirect.com/science/article/pii/S0378775310016952

Chen, T., Wang, W. G., Miao, H., Li, T., & Xu, C. (2011). Evaluation of carbon deposition behavior on the nickel/yttrium-stabilized zirconia anode-supported fuel cell fueled with simulated syngas. *J. Power Sources, 196*(5), 2461-2468. Retrieved from http://www.sciencedirect.com/science/article/pii/S0378775310020860

Cheng, Z., & Liu, M. (2007). Characterization of sulfur poisoning of Ni-YSZ anodes for solid oxide fuel cells using in situ Raman microspectroscopy. *Solid State Ionics, 178*(13-14), 925-935. Retrieved from http://www.sciencedirect.com/science/article/pii/S0167273807001385

Dong, J., Cheng, Z., Zha, S., & Liu, M. (2006). Identification of nickel sulfides on Ni-YSZ cermet exposed to H2 fuel containing H2S using Raman spectroscopy. *J. Power Sources, 156*(2), 461-465. Retrieved from http://www.sciencedirect.com/science/article/pii/S0378775305008724

Drewery, M., Kennedy, E., Alenazey, F., Dlugogorski, B., & Stockenhuber, M. (2015). The effect of synthesis gas composition on the performance of Ni-based solid oxide fuel cells. *Chem. Eng. Res. Des., 101*, 22-26. Retrieved from http://www.sciencedirect.com/science/article/pii/S0263876215002531

Fan, P., Zhang, X., Hua, D., & Li, G. (2016). Experimental Study of the Carbon Deposition from CH4 onto the Ni/YSZ Anode of SOFCs. *Fuel Cells, 16*(2), 235-243. Retrieved from http://dx.doi.org/10.1002/fuce.201500038

Hagen, A. (2013). Sulfur Poisoning of the Water Gas Shift Reaction on Anode Supported Solid Oxide Fuel Cells. *Journal of The Electrochemical Society, 160*(2), F111-F118. Retrieved from http://jes.ecsdl.org/content/160/2/F111.abstract

Hagen, A., Barfod, R., Hendriksen, P. V., Liu, Y.-L., & Ramousse, S. (2006). Degradation of Anode Supported SOFCs as a Function of Temperature and Current Load. *Journal of The Electrochemical Society, 153*(6), A1165-A1171. Retrieved from http://jes.ecsdl.org/content/153/6/A1165.abstract

Hagen, A., Johnson, G. B., & Hjalmarsson, P. (2014). Electrochemical evaluation of sulfur poisoning in a methane-fuelled solid oxide fuel cell: Effect of current density and sulfur concentration. *Journal of Power Sources, 272*, 776-785. Retrieved from http://www.sciencedirect.com/science/article/pii/S0378775314014001

Hagen, A., Rasmussen, J. F., & Thydén, K. (2011, #sep#). Durability of solid oxide fuel cells using sulfur containing fuels. *Journal of Power Sources, 196*(17), 7271-7276. Retrieved from http://www.sciencedirect.com/science/article/pii/S0378775311004800

Hauch, A., Hagen, A., Hjelm, J., & Ramos, T. (2014). Sulfur Poisoning of SOFC Anodes: Effect of Overpotential on Long-Term Degradation. *J. Electrochem. Soc., 161*(6), F734-F743. Retrieved from http://jes.ecsdl.org/content/161/6/F734.abstract

Hauch, A., Jørgensen, P. S., Brodersen, K., & Mogensen, M. (2011). Ni/YSZ anode - Effect of pre-treatments on cell degradation and microstructures. *J. Power Sources, 196*(21), 8931-8941. Retrieved from http://www.sciencedirect.com/science/article/pii/S0378775311000814

Hauch, A., Mogensen, M., & Hagen, A. (2011). Ni/YSZ electrode degradation studied by impedance spectroscopy - Effect of p(H2O). *Solid State Ionics, 192*(1), 547-551. Retrieved from http://www.sciencedirect.com/science/article/pii/S0167273810000056

He, H., & Hill, J. M. (2007). Carbon deposition on Ni/YSZ composites exposed to humidified methane. *Applied Catalysis A: General, 317*(2), 284-292. Retrieved from http://www.sciencedirect.com/science/article/pii/S0926860X06007757

Holzer, L., Iwanschitz, B., Hocker, T., Münch, B., Prestat, M., Wiedenmann, D., . . . Graule, T. (2011). Microstructure degradation of cermet anodes for solid oxide fuel cells: Quantification of nickel grain growth in dry and in humid atmospheres. *Journal of Power Sources, 196*(3), 1279-1294. Retrieved from http://www.sciencedirect.com/science/article/pii/S0378775310013352

Ivey, D. G., Brightman, E., & Brandon, N. (2010, #oct#). Structural modifications to nickel cermet anodes in fuel cell environments. *Journal of Power Sources, 195*(19), 6301-6311. Retrieved from http://www.sciencedirect.com/science/article/pii/S0378775310006944

Jørgensen, P., Ebbehøj, S., & Hauch, A. (2015). Triple phase boundary specific pathway analysis for quantitative characterization of solid oxide cell electrode microstructure. *J. Power Sources, 279*, 686-693. Retrieved from http://www.sciencedirect.com/science/article/pii/S037877531500066X

Jiao, Y., Zhang, L., An, W., Zhou, W., Sha, Y., Shao, Z., . . . Li, S.-D. (2016, #oct#). Controlled deposition and utilization of carbon on Ni-YSZ anodes of SOFCs operating on dry methane. *Energy, 113*, 432-443. Retrieved from http://www.sciencedirect.com/science/article/pii/S0360544216309872

Jiao, Z., & Shikazono, N. (2015). Quantitative Study on the Correlation between Solid Oxide Fuel Cell Ni-YSZ Composite Anode Performance and Reduction Temperature Based on Three-Dimensional Reconstruction. *J. Electrochem. Soc., 162*(6), F571-F578. Retrieved from http://jes.ecsdl.org/content/162/6/F571.abstract

Khan, M. S., Lee, S.-B., Song, R.-H., Lee, J.-W., Lim, T.-H., & Park, S.-J. (2016). Fundamental mechanisms involved in the degradation of nickel-yttria stabilized zirconia (Ni-YSZ) anode during solid oxide fuel cells operation: A review. *Ceram. Int., 42*(1, Part A), 35-48. Retrieved from http://www.sciencedirect.com/science/article/pii/S0272884215017149

Kishimoto, H., Horita, T., Yamaji, K., Brito, M. E., Xiong, Y.-P., & Yokokawa, H. (2010). Sulfur Poisoning on SOFC Ni Anodes: Thermodynamic Analyses within Local Equilibrium Anode Reaction Model. *Journal of The Electrochemical Society, 157*(6), B802-B813. Retrieved from http://jes.ecsdl.org/content/157/6/B802.abstract

Klotz, D., Butz, B., Leonide, A., Hayd, J., Gerthsen, D., & Ivers-Tiffée, E. (2011, #jun#). Performance Enhancement of SOFC Anode Through Electrochemically Induced Ni/YSZ Nanostructures. *J. Electrochem. Soc., 158*(6), B587--B595. Retrieved from http://jes.ecsdl.org/content/158/6/B587.abstract

Koh, J.-H., Yoo, Y.-S., Park, J.-W., & Lim, H. C. (2002). Carbon deposition and cell performance of Ni-YSZ anode support SOFC with methane fuel. *Solid State Ionics, 149*(3-4), 157-166. Retrieved from http://www.sciencedirect.com/science/article/pii/S0167273802002436

Kuhn, J., & Kesler, O. (2014, #jan#). Method for in situ carbon deposition measurement for solid oxide fuel cells. *J. Power Sources, 246*, 430-437. Retrieved from http://www.sciencedirect.com/science/article/pii/S0378775313013153

Kuhn, J., & Kesler, O. (2015). Carbon deposition thresholds on nickel-based solid oxide fuel cell anodes I. Fuel utilization. *Journal of Power Sources, 277*, 443-454. Retrieved from http://www.sciencedirect.com/science/article/pii/S037877531401129X

Kuhn, J., & Kesler, O. (2015). Carbon deposition thresholds on nickel-based solid oxide fuel cell anodes II. Steam:carbon ratio and current density. *Journal of Power Sources, 277*, 455-463. Retrieved from http://www.sciencedirect.com/science/article/pii/S0378775314011288

Lanzini, A., Guerra, C., Leone, P., Santarelli, M., Smeacetto, F., Fiorilli, S., . . . Brandon, N. (2016, #feb#). Influence of the microstructure on the catalytic properties of SOFC anodes under dry reforming of methane. *Materials Letters, 164*, 312-315. Retrieved from http://www.sciencedirect.com/science/article/pii/S0167577X1530817X

Lanzini, A., Leone, P., Guerra, C., Smeacetto, F., Brandon, N., & Santarelli, M. (2013). Durability of anode supported Solid Oxides Fuel Cells (SOFC) under direct dry-reforming of methane. *Chemical Engineering Journal, 220*, 254-263. Retrieved from http://www.sciencedirect.com/science/article/pii/S1385894713000375

Lee, W. Y., Hanna, J., & Ghoniem, A. F. (2013, #jan#). On the Predictions of Carbon Deposition on the Nickel Anode of a SOFC and Its Impact on Open-Circuit Conditions. *Journal of The Electrochemical Society, 160*(2), F94--F105. Retrieved from http://jes.ecsdl.org/content/160/2/F94.abstract

Li, T. S., Xu, M., Gao, C., Wang, B., Liu, X., Li, B., & Wang, W. G. (2014). Investigation into the effects of sulfur on syngas reforming inside a solid oxide fuel cell. *J. Power Sources, 258*, 1-4. Retrieved from http://www.sciencedirect.com/science/article/pii/S0378775314002250

Lin, Y., Zhan, Z., & Barnett, S. A. (2006). Improving the stability of direct-methane solid oxide fuel cells using anode barrier layers. *Journal of Power Sources, 158*(2), 1313-1316. Retrieved from http://www.sciencedirect.com/science/article/pii/S0378775305014060

Lin, Y., Zhan, Z., Liu, J., & Barnett, S. A. (2005). Direct operation of solid oxide fuel cells with methane fuel. *Solid State Ionics, 176*(23-24), 1827-1835. Retrieved from http://www.sciencedirect.com/science/article/pii/S0167273805002407

Liu, J., & Barnett, S. A. (2003). Operation of anode-supported solid oxide fuel cells on methane and natural gas. *Solid State Ionics, 158*(1-2), 11-16. Retrieved from http://www.sciencedirect.com/science/article/pii/S0167273802007695

Lohsoontorn, P., Brett, D., & Brandon, N. (2008). The effect of fuel composition and temperature on the interaction of H2S with nickel-ceria anodes for Solid Oxide Fuel Cells. *Journal of Power Sources, 183*(1), 232-239. Retrieved from http://www.sciencedirect.com/science/article/pii/S0378775308007325

Macek, J., Novosel, B., & Marincek, M. (2007). Ni-YSZ SOFC anodes: Minimization of carbon deposition. *J. Eur. Ceram. Soc., 27*(2-3), 487-491. Retrieved from http://www.sciencedirect.com/science/article/pii/S0955221906002639

Manukyan, K. V., Avetisyan, A. G., Shuck, C. E., Chatilyan, H. A., Rouvimov, S., Kharatyan, S. L., & Mukasyan, A. S. (2015). Nickel Oxide Reduction by Hydrogen: Kinetics and Structural Transformations. *J. Phys. Chem. C, 119*(28), 16131-16138. Retrieved from http://dx.doi.org/10.1021/acs.jpcc.5b04313

Matsuzaki, Y., & Yasuda, I. (2000). The poisoning effect of sulfur-containing impurity gas on a SOFC anode: Part I. Dependence on temperature, time, and impurity concentration. *Solid State Ionics, 132*(3-4), 261-269. Retrieved from http://www.sciencedirect.com/science/article/pii/S0167273800006536

Miao, H., Liu, G., Chen, T., He, C., Peng, J., Ye, S., & Wang, W. G. (2015). Behavior of anode-supported SOFCs under simulated syngases. *J. Solid State Electrochem., 19*(3), 639-646. Retrieved from http://dx.doi.org/10.1007/s10008-014-2640-7

Millichamp, J., Mason, T. J., Brandon, N. P., Brown, R. J., Maher, R. C., Manos, G., . . . Brett, D. J. (2013, #aug#). A study of carbon deposition on solid oxide fuel cell anodes using electrochemical impedance spectroscopy in combination with a high temperature crystal microbalance. *Journal of Power Sources, 235*, 14-19. Retrieved from http://www.sciencedirect.com/science/article/pii/S037877531300267X

Noponen, M., Halinen, M., Kiviaho, J., & Saarinen, J. (2006). Feasibility of Autothermally Reformed Natural Gas on Anode Supported Solid Oxide Fuel Cells. *Journal of Fuel Cell Science and Technology, 3*(4), 438-444. Retrieved from http://dx.doi.org/10.1115/1.2349526

Papurello, D., Lanzini, A., Fiorilli, S., Smeacetto, F., Singh, R., & Santarelli, M. (2016). Sulfur poisoning in Ni-anode solid oxide fuel cells (SOFCs): Deactivation in single cells and a stack. *Chemical Engineering Journal, 283*, 1224-1233. Retrieved from http://www.sciencedirect.com/science/article/pii/S1385894715011730

Ploner, A., Hagen, A., & Hauch, A. (In Press). Study of Operating Parameters for Accelerated Anode Degradation in SOFCs. *Fuel Cells*.

Rasmussen, J. F., & Hagen, A. (2009). The effect of H2S on the performance of Ni-YSZ anodes in solid oxide fuel cells. *Journal of Power Sources, 191*(2), 534-541. Retrieved from http://www.sciencedirect.com/science/article/pii/S037877530900192X

Rasmussen, J. F., & Hagen, A. (2010). The Effect of H2S on the Performance of SOFCs using Methane Containing Fuel. *Fuel Cells, 10*(6), 1135-1142. Retrieved from http://dx.doi.org/10.1002/fuce.201000012

Rostrup-Nielsen, J., Hansen, J., Helveg, S., Christiansen, N., & Jannasch, A.-K. (2006). Sites for catalysis and electrochemistry in solid oxide fuel cell (SOFC) anode. *Applied Physics A, 85*(4), 427-430. Retrieved from http://dx.doi.org/10.1007/s00339-006-3702-1

Sasaki, K., & Teraoka, Y. (2003, #jul#). Equilibria in Fuel Cell Gases: II. The C-H-O Ternary Diagrams. *Journal of The Electrochemical Society, 150*(7), A885--A888. Retrieved from http://jes.ecsdl.org/content/150/7/A885.abstract

Sasaki, K., Susuki, K., Iyoshi, A., Uchimura, M., Imamura, N., Kusaba, H., . . . Jingo, N. (2006). H2S Poisoning of Solid Oxide Fuel Cells. *Journal of The Electrochemical Society, 153*(11), A2023-A2029. Retrieved from http://jes.ecsdl.org/content/153/11/A2023.abstract

Shiratori, Y., Ijichi, T., Oshima, T., & Sasaki, K. (2010). Internal reforming SOFC running on biogas. *International Journal of Hydrogen Energy, 35*(15), 7905-7912. Retrieved from http://www.sciencedirect.com/science/article/pii/S0360319910010165

Smith, T. R., Wood, A., & Birss, V. I. (2009). Effect of hydrogen sulfide on the direct internal reforming of methane in solid oxide fuel cells. *Applied Catalysis A: General, 354*(1-2), 1-7. Retrieved from http://www.sciencedirect.com/science/article/pii/S0926860X08006674

Snoeck, J.-W., Froment, G. F., & Fowles, M. (2002, #aug#). Steam/CO2 Reforming of Methane. Carbon Filament Formation by the Boudouard Reaction and Gasification by CO2, by H2, and by Steam: Kinetic Study. *Ind. Eng. Chem. Res., 41*(17), 4252-4265. Retrieved from http://dx.doi.org/10.1021/ie010666h

Subotic, V., Schluckner, C., Mathe, J., Rechberger, J., Schroettner, H., & Hochenauer, C. (2015, #nov#). Anode regeneration following carbon depositions in an industrial-sized anode supported solid oxide fuel cell operating on synthetic diesel reformate. *Journal of Power Sources, 295*, 55-66. Retrieved from http://www.sciencedirect.com/science/article/pii/S0378775315300239

Subotic, V., Schluckner, C., Stöckl, B., Lawlor, V., Schroettner, H., & Hochenauer, C. (2016, #jan#). Strategy for Carbon Gasification from Porous Ni-YSZ Anodes of Industrial-Sized ASC-SOFCs and Effects of Carbon Growth. *Journal of The Electrochemical Society, 163*(14), F1515--F1522. Retrieved from http://jes.ecsdl.org/content/163/14/F1515.abstract

Subotic, V., Schluckner, C., Strasser, J., Lawlor, V., Mathe, J., Rechberger, J., . . . Hochenauer, C. (2016, #jul#). In-situ electrochemical characterization methods for industrial-sized planar solid oxide fuel cells Part I: Methodology, qualification and detection of carbon deposition. *Electrochim. Acta, 207*, 224-236. Retrieved from http://www.sciencedirect.com/science/article/pii/S0013468616310714

Szász, J., Seils, S., Klotz, D., Störmer, H., Heilmaier, M., Gerthsen, D., . . . Ivers-TiffÃ©e, E. (2017, #may#). High Resolution Studies on Nanoscaled Ni/YSZ Anodes. *Chem Mater*, --. Retrieved from http://dx.doi.org/10.1021/acs.chemmater.7b00360

Takeguchi, T., Kani, Y., Yano, T., Kikuchi, R., Eguchi, K., Tsujimoto, K., . . . Aizawa, M. (2002). Study on steam reforming of CH4 and C2 hydrocarbons and carbon deposition on Ni-YSZ cermets. *J. Power Sources, 112*(2), 588-595. Retrieved from http://www.sciencedirect.com/science/article/pii/S0378775302004718

Takenaka, S., Kato, E., Tomikubo, Y., & Otsuka, K. (2003). Structural change of Ni species during the methane decomposition and the subsequent gasification of deposited carbon with CO2 over supported Ni catalysts. *J. Catal., 219*(1), 176-185. Retrieved from http://www.sciencedirect.com/science/article/pii/S0021951703001520

Takenaka, S., Shimizu, T., & Otsuka, K. (2004, #aug#). Complete removal of carbon monoxide in hydrogen-rich gas stream through methanation over supported metal catalysts. *Int. J. Hydrogen Energy, 29*(10), 1065-1073. Retrieved from http://www.sciencedirect.com/science/article/pii/S0360319903003070

Takenaka, S., Tomikubo, Y., Kato, E., & Otsuka, K. (2004). Sequential production of H2 and CO over supported Ni catalysts. *Fuel, 83*(1), 47-57. Retrieved from http://www.sciencedirect.com/science/article/pii/S0016236103002114

Thydén, K. (2008). *Microstructural degradation of Ni-YSZ anodes for solid oxide fuel cells.* Ph.D. dissertation, Technical University of Denmark.

Triantafyllopoulos, N. C., & Neophytides, S. G. (2003). The nature and binding strength of carbon adspecies formed during the equilibrium dissociative adsorption of CH4 on Ni-YSZ cermet catalysts. *J. Catal., 217*(2), 324-333. Retrieved from http://www.sciencedirect.com/science/article/pii/S0021951703000629

Weber, A., Dierickx, S., Kromp, A., & Ivers-Tiffee, E. (2013). Sulfur Poisoning of Anode-Supported SOFCs under Reformate Operation. *Fuel Cells, 13*(4), 487-493. Retrieved from http://dx.doi.org/10.1002/fuce.201200180

Yang, L., Cheng, Z., Liu, M., & Wilson, L. (2010). New insights into sulfur poisoning behavior of Ni-YSZ anode from long-term operation of anode-Supported SOFCs. *Energy & Environmental Science, 3*, 1804-1809. Retrieved from http://pubs.rsc.org/en/Content/ArticleLanding/2010/EE/c0ee00386g#!divAbstract

Yoshizumi, T., Taniguchi, S., Shiratori, Y., & Sasaki, K. (2012). Sulfur Poisoning of SOFCs: Voltage Oscillation and Ni Oxidation. *Journal of The Electrochemical Society, 159*(11), F693-F701. Retrieved from http://jes.ecsdl.org/content/159/11/F693.abstract

Zha, S., Cheng, Z., & Liu, M. (2007, #feb#). Sulfur Poisoning and Regeneration of Ni-Based Anodes in Solid Oxide Fuel Cells. *Journal of The Electrochemical Society, 154*(2), B201--B206. Retrieved from http://jes.ecsdl.org/content/154/2/B201.abstract

Zhang, Y., Yang, Z., & Wang, M. (2015, #apr#). Understanding on the carbon deposition on the Nickel/Yttrium-Stabilized Zirconia anode caused by the CO containing fuels. *Journal of Power Sources, 279*, 759-765. Retrieved from http://www.sciencedirect.com/science/article/pii/S0378775315000865

5. Cathode review :

5.1. O_2 electrode destabilization in SOFC vs SOEC mode (Process: Cath1, Cath2)

Extracted from: Laurencin, J., Hubert, M., Sanchez, D.F., Pylypko, S., Morales, M., Morata, A., Morel, B., Montinaro, D., Lefebvre-Joud, F., Siebert, E., 2017. Degradation mechanism of $La_{0.6}Sr_{0.4}Co_{0.2}Fe_{0.8}O_{3-\delta}/Gd_{0.1}Ce_{0.9}O_{2-\delta}$ composite electrode operated under solid oxide electrolysis and fuel cell conditions. Electrochimica Acta 241, 459–476. doi:10.1016/j.electacta.2017.05.011

The O_2 electrode is currently made of Mixed Ionic Electronic Conductors (MIECs) such as Lanthanum Strontium Cobalt (LSC) or Lanthanum Strontium Cobalt Ferrite (LSCF). A thin barrier layer of Ceria doped Gadolinium Oxide (CGO) is usually added between LSCF or LSC and YSZ to mitigate material reactivity at high temperatures. Besides, LSCF-CGO composite has been recently proposed to replace the LSCF or LSC single-phase electrode in order to improve the mechanical compatibility with the electrolyte [1]. It seems that such composite could also enhance the cell performances when it is operated in electrolysis mode [2].

Nevertheless, the durability of the SOCs is nowadays one of the main issues of the technology. Indeed, the degradation rates recorded on stacks tested in real conditions of operation are still too high. Economic viability would be achieved for a degradation limited to few tenths of percent per khrs (<0.5%/khrs) [3]. However, typical degradation rates of ~1%/khrs [1,4] and ~2-3%/khrs [4-6] are currently reported in fuel cell and electrolysis operating modes respectively. These degradations are mainly attributed to electrode microstructural evolutions [7,8], electro-active sites poisoning by contaminants [9], material chemical decomposition [10] associated with inter-diffusion, and reactivity between cell components [11]. Among all these phenomena, several studies have indicated that LSCF or LSC destabilization could be one of the main contribution to the global cell degradation [12]. For cells tested in SOEC mode with a LSCF oxygen electrode and a CGO interlayer, The et al. [13] have detected the perovskite phase **demixing** which is accompanied with the formation of a **$SrZrO_3$** (SZO) insulating phase within the barrier layer. In SOFC mode, Endler et al. [12] have given evidences that the performance loss would be essentially influenced by the electrode **LSCF degradation**. Tietz et al. [14] have also claimed that the SOFC voltage loss would be mainly caused by the **slow decomposition of LSCF**. Long-term tests have been also performed on LSCF-CGO composite electrode in fuel cell operating condition by Kiebach et al. [15] and Liu et al. [16]. For screen printed cathode sintered at 1250°C, Kiebach et al. [15] have found that LSCF phase demixing and $SrZrO_3$ formation occur mainly during the cell **manufacturing** process whereas their contributions to the long-term degradation can be neglected. At the contrary, for LSCF-CGO cathode prepared by impregnation and calcined at rather low temperature (800°C), Liu et al. [16] have found that LSCF **destabilization** contributes to the voltage loss over time. Therefore, it worth mentioning that $SrZrO_3$ formation in operation and its impact on the electrochemical degradation strongly depend on the electrode manufacturing route.

Despite many studies, the precise mechanism of destabilization for LSCF or LSC perovskite-type electrode is still not fully understood. Nevertheless, several experimental works have clearly established that **Sr tends to segregate at the surface** of the MIEC particles in operation [17-20]. The segregation of Sr^{2+} cations would be driven by a combination of **surface charge minimization and a strain relaxation of the host lattice** [21]. It has been postulated that surface Sr segregation should lead to the formation of a **SrO passivation film onto the LSCF** particles [17,18,22]. For the $La_{0.6}Sr_{0.4}Co_{0.2}Fe_{0.8}O_{3-\delta}$ perovskite, Oh et al. [19] have clearly identified the precipitation of strontium-oxide based compound after heat treatment in the temperature range of 600–900°C, whereas Liu et al. [16] have detected the formation of $SrCoO_x$ particles after cathodic polarization at 750°C. Cai et al. [23] have found the presence of **SrO and $Sr(OH)_2$** species on the surface of a $La_{0.6}Sr_{0.4}Co_{0.3}O_{3-\delta}$ cathode thin film. Surface Sr segregation and formation of SrO and

$Sr(OH)_2$ phases are clearly related to the subsequent reactivity and apparition of **$SrZrO_3$** secondary phase within the CGO barrier layer [21]. As suggested by Tietz et al. [14], the **strontium** mass transport from the electrode to the CGO barrier layer probably occurs in the **gas phase** with the $Sr(OH)_2$ volatile specie. Indeed, the gaseous mass transfer of Sr could explain why **fully dense CGO barrier layers allows suppressing the formation of $SrZrO_3$** at typical SOFC/SOEC operating temperatures (T<800°C) [11,18,24].

A number of experiments have clearly demonstrated that Sr accumulation and formation of Sr-O based compounds on the surface induce the degradation in the electrode performances [17,18,20,22]. As an illustration, Kubicek et al. [22] have found that **chemical etching of aged electrodes allows removing the Sr** enriched layer and hence, to recover the electrode performances. To explain such a behavior, it has been suggested [17,23] that the growth of a SrO passivation film on the electrode surface [25] and the subsequent formation of $Sr(OH)_2$ adsorbed product should be detrimental for the oxygen reaction rate (adsorption/desorption, surface diffusion and incorporation/excorporation [26]). This statement is quite in good agreement with conductivity relaxation measurements which have highlighted a decrease at 600°C of the chemical surface exchange coefficient over time [27]. Conversely to the surface Sr segregation, it remains unclear if the formation of $SrZrO_3$ within the barrier layer could also participate to the performance deterioration. However, it has been found that **dense CGO** barrier layer, which allows suppressing the $SrZrO_3$ reactivity at SOFC/SOEC operating temperature, **does not contribute to improve the cell durability** [24]. Based on this finding, it has been suggested by Tietz et al. [14] that the perovskite **decomposition** should have **more influence on the electrochemical degradation than the interfacial reaction**.

To date, few studies have been devoted to assess the **impact of the operating conditions on the LSCF or LSC destabilization**. Some contradictory results have even been reported in the literature so that the effect of the operating conditions on the material demixing and $SrZrO_3$ formation needs to be clarified. For instance, Endler-Schuck et al. [28] have claimed that the LSCF degradation increases with decreasing the operating **temperature**; whereas, Oh et al. [19] have found that formation of Sr-O precipitates increases with increasing the temperature. The effect of electrode **polarization** is also unclear. On a chromium doped Lanthanum Strontium Manganate (LSCrM), Huber et al. [29] and Rohnke et al. [30] have found that the **cathodic** polarization (SOFC mode) **decreases** the surface Sr concentration while the **anodic** polarization (SOEC mode) increases the Sr accumulation at the surface. These results seem to be consistent with Wang et al. [31] and Baumann et al. [32] who have reported an **electrochemical activation by applying a cathodic bias** (on a doped Lanthanum Strontium Manganite (LSM) and a LSCF electrode, respectively). However, these statements are **inconsistent** with the studies of Pan et al. [17,33] who have reported on a LSCF electrode that a passage under **anodic current can regenerate the electrode performances after ageing**. Conversely to the temperature and polarization, it seems rather well established that **higher water** content in the gas [27,34] **enhances the LSCF demixing**. This would suggest to perform specific experiments to regenerate LSCF, e.g. by a low PO_2 treatment (5% O_2).

A set of long-term tests (t>1000 h) have been carried out in fuel cell and electrolysis modes on typical Ni-YSZ//YSZ//LSCF-CGO cells. The degradation rates were found to be higher in electrolysis than in fuel cell operation. Post-test analyses have revealed that Sr diffusion and **formation of $SrZrO_3$** at YSZ/CGO interface occur mainly during electrolysis operation, whereas the **process is very limited in fuel cell mode**. As a consequence, LSCF destabilization is found to be not involved in the degradation of cell performances during fuel cell operation while it could explain the highest degradation rates recorded in electrolysis mode. An in-house multi-scale model has been used to interpret the role of the cell operating mode on the LSCF demixing mechanism. The simulations have shown that the electrolysis operation leads to a strong depletion of oxygen vacancies in LSCF material (while the fuel cell condition results in an increase in the concentration of oxygen vacancies). It has been proposed that the depletion in oxygen vacancies under electrolysis

polarization could drive the Sr release from the structure, and in turn, could explain the experimental results. Based on this proposition, a possible mechanism for the LSCF destabilization and $SrZrO_3$ formation is detailed.

Cathode bibliography

[1] P. Hjalmarsson, X. Sun, Y.-L. Liu, Ming Chen, J. Power Sources 262 (2014) 316– 322.
[2] M. Hubert, J. Laurencin, P. Cloetens, J.C. Da Silva, F. Lefebvre-Joud, P. Bleuet, A. Nakajo, E. Siebert, Solid State Ionics 294 (2016) 90–107.
[3] N. Mahato, A. Banerjee, A. Gupta, S. Omar, K. Balani, A review. Progress in Materials Science 72 (2015) 141–337.
[4] T.L. Skafte, J. Hjelm, P. Blennow, C. Graves, Quantitative review of degradation and lifetime of solid oxide cells and stacks, in: 12th European SOFC & SOE Forum, B0501, Lucerne, Switzerland, 2016.
[5] A. Hauch, D. Ebbensen, S.H. Jensen, M. Mogensen, J. Electrochem. Soc. 155 (11) (2008) B-1284-B1193.
[6] J. Schefold, A. Brisse, F. Tietz, J. Electrochem. Soc. 159 (2) (2012) A137–A144.
[7] E. Lay-Grindler, J. Laurencin, J. Villanova, P. Cloetens, P. Bleuet, A. Mansuy, J. Mougin, G. Delette, Journal of Power Sources 269 (2014) 927–936.
[8] D. Simwonis, F. Tietz, D. Stover, Solid State Ionics 132 (2000) 241–251.
[9] A. Hauch, H. Jensen, J.B. Bilde-Sørensen, M. Mogensen, J. Electrochem. Soc. 154 (2007) A619–A626.
[10] H. Yokokawa, N. Sakai, T. Kawada, M. Dokiya, Solid State Ionics 52 (1992) 43– 56.
[11] S. Uhlenbruck, T. Moskalewicz, N. Jordan, H.-J. Penkalla, H.P. Buchkremer, Solid State Ionics. 180 (2009) 418–423.
[12] C. Endler, A. Leonide, A. Weber, F. Tietz, E. Ivers-Tiffée, J. Electrochem. Soc. 157 (2) (2010) B292–B298.
[13] D. The, S. Grieshammer, M. Schroeder, M. Martin, M. Al Daroukh, F. Tietz, J. Shefold, A. Brisse, J. Power Sources 275 (2015) 901–911.
[14] F. Tietz, A. Mai, D. Stöver, Solid State Ionics 179 (2008) 1509–1515.
[15] R. Kiebach, W.-W. Zhang, W. Zhang, M. Chen, K. Norrman, H.-J. Wang, J.R. Bowen, R. Barfod, P.V. Hendriksen, J. Power Sources 283 (2015) 151–161.
[16] Y. Liu, K. Chen, L. Zhao, B. Chi, J. Pu, S.P. Jiang, L. Jian, Int. J. Hydrogen Energy 39 (2014) 15868–15876.
[17] Z. Pan, Q. Liu, L. Zhang, X. Zhang, S.H. Chan, J. Electrochem. Soc. 162 (12) (2015) F1316–F1323.
[18] H. Wang, K.J. Yakal-Kremski, T. Yeh, G.M. Rupp, A. Limbeck, J. Fleig, S.A. Barnett, J. Electrochem. Soc. 163 (6) (2016) F581–F585.
[19] D. Oh, D. Gostovic, E.D. Wachsman, J. Mater. Res. 27 (15) (2012) 1992–1999.
[20] S.P. Simner, M.D. Anderson, M.H. Engelhard, J.W. Stevenson, Electrochem. Solid State Letters 9 (10) (2006) A478–A481.
[21] H. Ding, A.V. Virkar, M. Liu, F. Liu, Phys. Chem. Chem. Phys. 15 (2013) 489–496.
[22] M. Kubicek, A. Limbeck, T. Frömling, H. Hutter, J. Fleig, J. Electrochem. Soc. 158 (6) (2011) B727–B734.
[23] Z. Cai, M. Kubicek, J. Fleig, B. Yildiz, Chem. Mater. 24 (2012) 1116–1127.
[24] F. Tietz, Q.X. Fu, V.A.C. Haanappel, A. Mai, N.H. Menzler, S. Uhlenbruck, Inter. J. Appl. Ceram. Technol. 4 (5) (2007) 436–445.
[25] W.D. Copeland, R.A. Swalin, J. Phys. Chem. Solids 29 (1968) 313–325.
[26] J. Laurencin, M. Hubert, K. Couturier, T. Le Bihan, P. Cloetens, F. Lefebvre-Joud, E. Siebert, Electrochim. Acta 174 (2015) 1299–1316.
[27] E. Bucher, W. Sitte, Solid State Ionics 192 (2011) 480–482.
[28] C. Endler-Schuck, A. Leonide, A. Weber, S. Uhlenbruck, F. Tietz, E. Ivers-Tiffée, J. Power Sources 196 (2011) 7257–7267.
[29] A.-K. Huber, M. Falk, M. Rohnke, B. Luerßen, L. Gregoratti, M. Amati, J. Janek, Phys. Chem. Chem. Phys. 14 (2012) 751–758.
[30] M. Rohnke, M. Falk, A.-K. Huber, J. Janek, J. Power Sources 221 (2013) 97–107.
[31] W. Wang, S.P. Jiang, Solid State Ionics 177 (2006) 1361–1369.
[32] F.S. Baumann, J. Fleig, M. Konuma, U. Starke, H.-U. Habermeier, J. Maier, J. Electrochem. Soc. 152 (10) (2005) A2074–A2079.
[33] Z. Pan, Q. Liu, L. Zhang, X. Zhang, S.H. Chan, Electrochimica Acta 209 (2016) 56– 64.
[34] P. Hjalmarsson, M. Sogaard, M. Mogensen, Solid State Ionics 179 (2008) 1422– 1426.

6. Sealing degradation overview (Process: Seal1, Seal2)

6.1 Sealing materials

The different types of sealing solutions for planar SOFC stacks can be divided into rigid seals, compressible seals and hybrid seals. Rigid seals consist of glass/glass-ceramic sealants and metallic brazes which do not require high compression forces to achieve gas tightness. [1] For SOFC applications, alkaline-earth-based glasses are preferred. Alkali-metal glasses are also used but generally avoided in SOFC applications since alkali-metal species react with SOFC materials and can also enhance the volatility of chromium, which increase the risk of cathode chromium poisoning. [1,2]

Compressible gaskets can be made of mineral paper, such as phologipite mica paper (tradenames e.g. Statotherm HT and Cogemina) or combination of different materials, such as exfoliated vermiculite mixed with steatite (talk) (Thermiculite, Flexitallic Ltd) [3,4]. Another type of compressible gaskets are alumina felt (sold by fuelcellmaterials.com, NextTech Materials Ltd). Compressible gaskets require a higher compression force but can be more stable against thermal cycling than glass / glass-ceramics, which often are brittle.

Hybrid seals consist either of a core of compressible sealing material with adjacent glass layers on both sides or of a mixture of glass and compressible sealing material. Such sealing solutions often show low leak rates at comparatively low compression forces and withhold still a degree of formability. [5–7]

Metallic seals and brazes are possible sealing solutions in locations where electrical conductivity is desired. To achieve insulating seals, another insulating layer must be added to form a composite gasket. Non-oxidizing materials such as Au and Ag have been tested as flat gaskets and metals such as Ag, Au, Cu, Ni, Ti, etc., and alloys of these, have been tested for brazes. Brazes generally have a lower melting point than the stack operation conditions and wets and joins therefore the adjacent materials (ceramics, metals) without modifying these. The thermal expansion coefficient of brazing material must be very close to that of the ceramic materials to be joined, such as YSZ, to avoid cracking the cells. [2,8–10]

6.2 Degradation modes and detection

Degradation phenomena related to seals and their recovery potential depend to a certain degree on the type of sealing solution used. Sealing related degradation can be divided into the following failure modes:

1. Increased **leak rates** in stack (cross-leak or to outside)
2. **Mechanical failure of seal** or adjacent components (e.g. loss of contact pressure in case of compressible seals or thermomechanically induced cracking of glass-ceramic seals)
3. **Chemical instability of sealing** material with adjacent components (sealing material causes or increases corrosion at its' interfaces)
4. **Released species from sealing** material contributing to the electrochemical degradation of the cell

Failures of gas tightness can arise due to rapid **thermal cycling, thermal aging, loss of gasket rigidity, creep or fracturing** of the seal under pressurization, thus calling for well-planned stack operation. [11] Internal leakages consume fuel and lead to higher fuel utilization and lower stack performance. The combustion of fuel on the leak location can also create a **hot spot**, i.e. a location with a highly elevated temperature, leading to further degradation of stack components. The increased **humidity** from fuel combustion may also increase **corrosion of ferritic stainless steel** used for interconnect plates as well as **increased chromium evaporation** from ICs, leading to chromium poisoning of cathodes [12–14]. Internal leakages can be **detected by a decrease in the open cell** voltage according to the Nernst equation and often by an **increase in outlet air humidity**, due to combustion of fuel on cathode side.

6.3 Recovery

Recovery possibilities depend on the type of seal. One solution is to **increase the stack compression**. However, compressible mica sealants lose their compressibility already at 200 °C, since the material dries and becomes hard. The compressibility of Thermiculite 866 decreased from 40% at room temperature to 4% between 0.1 and 0.9 MPa [15].

Cracks through glass / glass-ceramic seals could possibly **recover by self-healing**, i.e. upon **heating** to sufficiently high temperatures, the glass flows and fills the crack. Suitable glass transition and softening temperature, viscosity and a stability against crystallization are required for such glasses. [11,16] With such glasses, an increase in temperature could decrease the leak. Increase of compression should be used carefully since there is a risk of pressing the glass material into gas channels etc., thus obstructing gas flow in the stack.

Mechanical failure modes related to sealing materials can include e.g. excessive creep of compressible sealing materials, cracking of glass-ceramic materials or thermo-mechanical stresses induced to adjacent components and stack structures. Loss of contact pressure on the compressible seals transfers more loading on the cell and other components of the stack, which may cause e.g. deformation of interconnects or cracking of cells.

Another type of degradation can arise from **contaminations** in the sealing material or from sealing components themselves. It was already noted that alkali-metal based glasses could increase chromium volatility and poisoning [1]. Also other glass components, such as **barium** in barium aluminosilicate glasses tend to react with **chromium** and form reaction products that becomes porous and susceptible to cracking in long-term [2,17]. Batfalsky et al reported on minor amounts of **PbO** in glass-ceramic sealants to cause corrosion, especially on steels with high Si content [18]. Another type of glasses, borosilicate-based glasses, are common as sealant materials in SOFC applications, but **boron has a high volatility** in SOFC operation conditions and volatile boron species act as **poisonous** species, thus degrading LSM and LSCF cathodes by degrading the microstructure and by formation of insulating borate phases [19,20].

Poisoning of the anode or cathode can detected by EIS but the exact mechanism is hard to distinguish from other electrode poison sources. **No recovery potential once the electrodes are poisoned**.

6.4 Mitigation / Preventing sealing material based degradation:

The following general guidelines serve to preventively minimize stack degradation induced by the sealing material:

1. Ensure **constant and sufficient compressive stress** on the sealing material throughout stack lifetime, taking into account creep of other components.
2. **Evaluate chemical stability of sealing** materials with adjacent components over operating atmospheres and temperature range.
3. By stack design, **minimize gas pressure differences** between anode and cathode and surroundings.
4. Ensure **homogeneous AU & FU** over the cell to minimize effects of leaks to local stack FU & AU.
5. **Minimize thermal expansion coefficient mismatch** between sealing materials and other stack parts, especially with glass-ceramics.

6.5 Summary on mitigation and recovery actions

In general, sealing failures can be mitigated by **minimizing the pressure difference** between the anode and cathode side of the stack, as well as between the stack and external atmosphere. **Heating and cooling rates** should be held sufficiently **slow** to avoid cracking of sealing material due to thermal stress.

Some types of compressible gaskets, such as alumina felt, could be further compressed to recover from a leak but mineral papers become hard after heating and are not possible to compress further. **Self-healing glass** materials have a potential to fill cracks within the glass by viscous flow upon increase of temperature.

6.6 Sealing Bibliography

[1] J.W. Fergus, Sealants for solid oxide fuel cells, J. Power Sources. 147 (2005). doi:10.1016/j.jpowsour.2005.05.002.

[2] K.S. Weil, The state-of-the-art in sealing technology for solid oxide fuel cells, JOM. 58 (2006).

[3] J.R. Hoyes, S. Bond, Gaskets for sealing solid oxide fuel cells, Seal. Technol. (2007). doi:10.1016/S1350-4789(07)70376-8.

[4] M. Rautanen, O. Himanen, V. Saarinen, J. Kiviaho, Compression properties and leakage tests of mica-based seals for SOFC stacks, Fuel Cells. 9 (2009). doi:10.1002/fuce.200900029.

[5] M. Rautanen, O. Thomann, O. Himanen, J. Tallgren, J. Kiviaho, Glass coated compressible solid oxide fuel cell seals, J. Power Sources. 247 (2014) 243–248.

[6] Y.-S. Chou, J.W. Stevenson, L.A. Chick, Ultra-low leak rate of hybrid compressive mica seals for solid oxide fuel cells, J. Power Sources. 112 (2002). doi:10.1016/S0378-7753(02)00356-7.

[7] J.R. Hoyes, M. Rautanen, SOFC sealing with thermiculite 866 and thermiculite 866 LS, in: ECS Trans., 2013. doi:10.1149/05701.2365ecst.

[8] M.C. Tucker, C.P. Jacobson, L.C. De Jonghe, S.J. Visco, A braze system for sealing metal-supported solid oxide fuel cells, J. Power Sources. 160 (2006). doi:10.1016/j.jpowsour.2006.02.067.

[9] T. Bause, J. Malzbender, M. Pausch, T. Beck, L. Singheiser, Damage and failure of silver based ceramic/metal joints for sofc stacks, Fuel Cells. 13 (2013). doi:10.1002/fuce.201200181.

[10] N.H. Menzler, F. Tietz, S. Uhlenbruck, H.P. Buchkremer, D. Stöver, Materials and manufacturing technologies for solid oxide fuel cells, J. Mater. Sci. 45 (2010). doi:10.1007/s10853-010-4279-9.

[11] A.A. Reddy, D.U. Tulyaganov, V.V. Kharton, J.M.F. Ferreira, Development of bilayer glass-ceramic SOFC sealants via optimizing the chemical composition of glasses—a review, J. Solid State Electrochem. 19 (2015). doi:10.1007/s10008-015-2925-5.

[12] C. Gindorf, L. Singheiser, K. Hilpert, Chromium vaporisation from Fe, Cr base alloys used as interconnect in fuel cells, Steel Res. 72 (2001).

[13] S.P. Jiang, X. Chen, Chromium deposition and poisoning of cathodes of solid oxide fuel cells - A review, Int. J. Hydrogen Energy. 39 (2014) 505–531. doi:10.1016/j.ijhydene.2013.10.042.

[14] C. Key, J. Eziashi, J. Froitzheim, R. Amendola, R. Smith, P. Gannon, Methods to Quantify Reactive Chromium Vaporization from Solid Oxide Fuel Cell Interconnects, J. Electrochem. Soc. 161 (2014) C373–C381. doi:10.1149/2.0041409jes.

[15] M. Rautanen, V. Pulkkinen, J. Tallgren, O. Himanen, J. Kiviaho, Effects of the first heat up procedure on mechanical properties of solid oxide fuel cell sealing materials, J. Power Sources. 284 (2015) 511–516.

[16] R.N. Singh, Sealing technology for solid oxide fuel cells (SOFC), Int. J. Appl. Ceram. Technol. 4 (2007). doi:10.1111/j.1744-7402.2007.02128.x.

[17] D.U. Tulyaganov, A.A. Reddy, V.V. Kharton, J.M.F. Ferreira, Aluminosilicate-based sealants for SOFCs and other electrochemical applications - A brief review, J. Power Sources. 242 (2013). doi:10.1016/j.jpowsour.2013.05.099.

[18] P. Batfalsky, V.A.C. Haanappel, J. Malzbender, N.H. Menzler, V. Shemet, I.C. Vinke, R.W. Steinbrech, Chemical interaction between glass-ceramic sealants and interconnect steels in SOFC stacks, J. Power Sources. 155 (2006). doi:10.1016/j.jpowsour.2005.05.046.

[19] K. Chen, L. Fang, T. Zhang, S.P. Jiang, New zinc and bismuth doped glass sealants with substantially suppressed boron deposition and poisoning for solid oxide fuel cells, J. Mater. Chem. A. 2 (2014). doi:10.1039/c4ta02951h.

[20] K. Chen, S.P. Jiang, Review - Materials degradation of solid oxide electrolysis cells, J. Electrochem. Soc. 163 (2016). doi:10.1149/2.0101611jes.

7. Metal Interconnect degradation review (Process : MIC1, MIC2)

Extracted from: Solid Oxide Fuel Cell Lifetime and Reliability. DOI: http://dx.doi.org/10.1016/B978-0-08-101102-7.00007-6. Chapter 7: Lifetime Issues for Solid Oxide Fuel Cell Interconnects. Manuel Bianco, Markus Linder, Yngve Larring, Fabio Greco and Jan Van herle.

7.1 Introduction

A SOFC interconnect must accomplish different tasks: divide cathode (air) and anode (fuel) streams (*gas impermeability*), distribute gas flows to optimize fuel utilization (*easy machining, stamping,..*), collect electrical current (*low electrical contact resistivity* < *10 mΩ·cm²*), guarantee mechanical stability (*creep resistance*), show sufficient chemical stability and inertia with respect to the other components (*low corrosion*), avoid residual stress potentially damaging to the ceramic cell (*coefficient of thermal expansion CTE compatible with the cell 12-13·10⁻⁶ K⁻¹* [1]), and transfer heat from the cathode to the anode in case of fuel reforming (*good thermal conductivity* > *5 Wm⁻¹K⁻¹* [2]).
Balancing all criteria leaves a limited choice of potential materials: $LaCrO_3$-based perovskites [3], Cr-based alloy, and **ferritic stainless steels** (FSS) [4], from higher to lower operating temperatures. No material completely fulfills all the features requested. The requirements for stationary applications -at least 40'000 hours at operating temperature- lead to interconnect lifetime issues such as mechanical deformation, corrosion, surface spallation, which impact the stack lifetime. To mitigate such processes, metal interconnects have specific chemical compositions and are combined with protective oxide coatings like a spinel or a perovskite layer deposited by different methods. The IC degradation mechanisms provide an important contribution to the overall stack degradation, especially after prolonged stack operation times (> 10'000 h). This is in turn due to improvements in electrodes' stability, and the fact that the major part of electrolyte degradation (a reduction in ionic conductivity) occurs within the first 4000 h [5].

Stainless steels are chosen for the anode-supported SOFC temperature regime because of their ability to grow a passivating oxide layer on the surface, preventing the formation of brittle and low electrically conductive hydrated iron oxide phases. The electrical insulating properties of aluminum oxide (σ_{Al2O3} ~10^{-10} S cm^{-1} @ 700°C [6]) leaves chromium oxide forming steel (σ_{Cr2O3} ~10^{-1} S cm^{-1} @ 750-800 °C [7][2]) as the appropriate choice for a SOFC interconnect [8]. The chromium content needed to ensure a continuous and homogeneous passivation layer is 18-19 wt.%, but considering the risk of Cr breakaway oxidation (depletion of the protecting element), 22-25 wt.% is considered a safer Cr content for the IC [4][8]. Following this, only austenitic (ASS) or ferritic (FSS) stainless steel is used in a SOFC stack, as martensitic stainless steel contains an insufficient amount of chromium. The austenitic phase is face-centered cubic while the ferritic phase is body-centered cubic. This difference causes different CTEs: 18-20·10^{-6} K^{-1} for the austenitic phase vs. 11-14 ·10^{-6} K^{-1} for the ferritic phase, in the SOFC temperature range of 25-800 °C [8], the FSS therefore being clearly much more compatible with the ceramic cell CTE (10.5-12.5·10^{-6} K^{-1} @ 30-800 °C [1]). On the other hand, ferritic stainless steel is less performing than austenitic steel in creep resistance and high temperature mechanical strength. High Cr-alloy also creates a protective passivating surface layer, and its CTE value is close to that of the cell (for Plansee CFY: 8.9-10.5 10^{-6} K^{-1} @ 300-800 °C [9]).
Different alloy compositions have been tested and improved in order to optimize for the property criteria mentioned above. The current state-of-the-art are specialized SOFC alloys: Crofer 22 APU or H, Sandvik Sanergy HT, Plansee ITM and CFY. In addition, commercial FSS grade AISI441/K41 is a widespread, SOFC non-specific alternative due to its lower cost, while it is less performing in corrosion resistance and mechanical properties. The alloy compositions are given in table 1.

Table 1. Elemental compositions of metal interconnect steels (weight%)

	K41/AISI 441 [10]	Sanergy HT [10]	Crofer 22 APU [11]	Crofer 22 H [10]	CFY [9]	IT-11 or ITM [12]
Fe	Bal.	Bal.	Bal.	Bal.	5.0	71.80
Cr	18.0	21.2	20.0-24.0	20.0-24.0	94.0	26.40
Y	-	-	-	-	1.0	0.08
C	0.012	0.04	0.0-0.03	0.0-0.03	-	0.009
Mn	0.30	0.30	0.30-0.80	0.0-0.80	-	-
Si	0.35	0.12	0.5	0.1-0.60	-	0.01
Al	-	0.017	0.5	0.0-0.10	-	0.02
Mo	-	0.96	-	-	-	-
Nb	0.45	0.71	-	0.2-1.0	-	-
Ti	0.17	0.09	0.03-0.20	0.02-0.20	-	-
W	-	-	-	1.0-3.0	-	-

7.2. Degradation processes

Corrosion and mechanical deformation are the most pronounced degradation phenomena. The former increases the electrical resistivity of the interconnect because of the poorer electrical conductivity of the thermally grown oxide layer, while the latter deforms the interconnect shape, potentially reducing the contact area with the cell.

Corrosion

Corrosion is [13] "the reaction of an engineering constructional metal (material) with its environment with a consequent deterioration in properties of the metal (material)". At microscopic level, corrosion is a two-step nucleation and growth process: oxidative species are adsorbed and react with the metal surface, starting oxide nucleation followed by two-dimensional lateral growth and finally a three-dimensional one. When the oxide layer is compact and continuous, growth becomes a diffusion-controlled phenomenon.
Based on the hypothesis of a diffusion-controlled process, Wagner developed a model based on Fick's law [14]. The scale thickness growth (Δx_{ox}) with time is proportional to a kinetic constant and follows a parabolic law:

$$\Delta x_{ox} = \sqrt[2]{K_p \cdot t} \qquad (1)$$

with K_p the corrosion or parabolic rate constant, explicitly defined as:

$$K_p = k \cdot \int_{p'_{O_2}}^{p''_{O_2}} D_M \, dln \, p_{O2} \qquad (2)$$

where k is a constant, D_M the diffusion coefficient for the dominant diffusive species, p'_{O_2} the oxygen partial pressure at the metal/oxide interface, and p''_{O_2} the oxygen partial pressure on top of the scale (for a detailed approach cf. [14][15][16]). Figure 1 gives an example for Cr_2O_3 scale growth on CFY interconnect cross sections at different time steps operated in SOFC stacks up to the first target lifetime of 40'000 h. The obtained scale growth for the investigated samples exhibits, more or less coincidentally, a parabolic behavior [17].

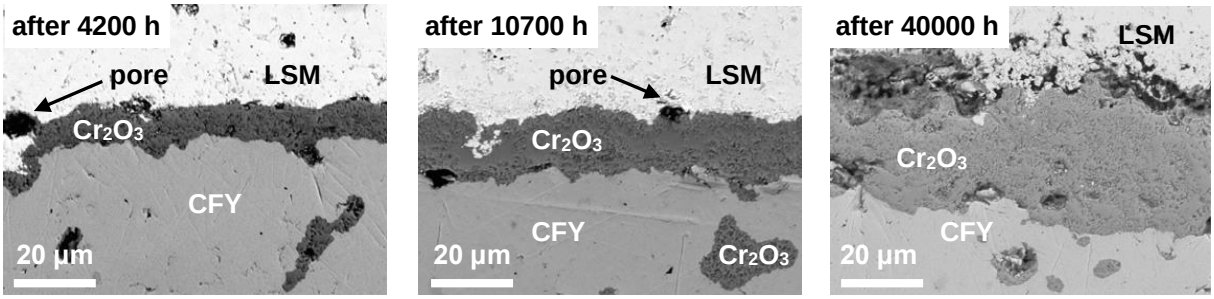

Figure 1. Oxide scale growth on CFY interconnects at the cathode side operated with air in Hexis SOFC stacks at 900 °C with CPOx reformed natural gas at the anode.

Correlation in equation (1) is *a priori* interesting because with a known K_p value obtained after a short experimental period of 1000 h, it is possible to predict the oxide layer thickness for longer periods, e.g. years (>10000 h). Such a minimal observation time is necessary because within the first few hundred hours of testing various interfering oxide formation mechanisms are involved in scale formation, which complicate a reliable **extrapolation** [18]. In addition, considering a simple model where the resistivity of the MIC is directly proportional to the scale thickness, **resistivity forecasting** is possible too. In reality, this basic approach is oversimplifying, when the fitted exponent *n* significantly deviates from purely parabolic behavior (*n*=0.5). Therefore other parameters must be taken into account, such as scale morphology, oxide scale composition (always containing various impurities) and transient operating conditions (e.g. redox and thermal cycles).

Comparing the evolution of the area specific resistance (ASR), from conductivity measurements, with the evolution of the Cr_2O_3 scale thickness, the trends are different and non-linear, with a much more pronounced variation at the beginning of exposure, i.e. for observation times < 5000 h. This behavior is related to the morphology of thermally grown oxide scales between the coating and the metallic substrate (on the cathode side). According to Ohm's law, the electrical current follows the paths of least resistance, which is necessarily through the bridges where the oxide scale is thinnest. These current bridges can lead to a significant reduction of ASR, considering that the electrical conductivity of the coatings and the IC is orders of magnitude higher than the formed Cr_2O_3. This provides local transversal electrical current pathways that amplify the bridging effect. Nevertheless, the impact of this bridging effect is time-dependent, in other words depending on the overall scale thickness. With increasing scale thickness the effect becomes less relevant, since the influence of the morphology effect, related to the measured ASR compared to the ASR predicted based on a uniform featureless oxide layer, decreases. The morphology factor $M(t)$ [19] is quantified based on a comprehensive amount of SEM images. For that purpose, the resulting $ASR_{\bar{x}}(t)$, derived from the mean oxide scale thickness, is set in relation to the calculated $ASR_{sim}(t)$, determined from finite element simulation:

$$M(t) = \frac{ASR_{\bar{x}}(t)}{ASR_{sim}(t)}.$$

Taking the morphology factor into account gives a significantly better fit with the experimentally determined ASR data, thus a more **reliable degradation prediction** based on oxide scale formation. Yet, even for M=1 the relation between scale thickness and resistivity is not straightforward: impurities and interaction with adjacent components, such as current pick-up mesh and coatings, influence the electrical conductivity of the Cr_2O_3-scale. Impurities dissolved in thermally grown Cr_2O_3-scales originate from alloying and/or the stack manufacturing process. This may improve the electrical conductivity of the formed oxide scale. Interaction with adjacent components can lead to the desirable formation of spinel phases like $(Cr,Mn)_3O_4$ or $NiCr_2O_4$.[20, 21]. Given this complex interplay it is obvious why sufficient testing time is essential for the reliable prediction of ASR trends and degradation [19].
Considering the alloys described in table 1, for equation (2) the majority diffusive species might be Cr^{3+} or O^{2-} ions, or their vacancies, with interstitial Cr-cations commonly accepted as the main diffusive species [15][16]. On the effect of oxygen partial pressure on K_p, there is no overall consensus. Most of the authors consider the oxidation rate to be independent of pO_2 [15, 22, 23], while others report

an interdependence [15]. A correlation between D_{Cr} and pO_2 at high temperature actually exists [22]. However, for small changes in oxygen partial pressure, like the condition existing at the SOFC cathode, D_{Cr} can be considered constant. The explanation for these different behaviors is not final.

Steam partial pressure influences the growth kinetics of the corrosion process. In general, K_p is found to increase in the **presence of humidity** both in anodic and cathodic conditions. Faster diffusion of ion hydroxide OH^- compared to O^{2-} (0.95 Å vs 1.4 Å ionic radius) through the scale is the prevailing accepted explanation for this [24]. At the same time, steam in the gas flows reacts with Cr_2O_3 producing at SOFC operating conditions the gas species $CrO_2(OH)_2$. This in turn depletes Cr from the steel and thins the scale. The predominance of one of the two processes is influenced by the deposition of a coating or by the alloy composition: for example, Mn migrates towards the alloy surface in the first stages of scale formation, forming a superficial $(Mn,Cr)_3O_4$ spinel layer that decreases Cr evaporation. Water vapor influences the structural scale properties: **porosity** in the thermally grown oxide layer is found to be more

homogenously distributed through the thickness, compared to a scale grown in a dry environment, where the pores are instead concentrated at the alloy/scale interface [24].

The aforementioned studies refer to samples studied in a single atmosphere. In a real stack the ICs work in a **dual atmosphere**. Experiments conducted with FSS alloys placed between reducing and oxidizing environments found a raise in Fe concentration in the thermally grown oxide layer at the air side, attributed to H proton migration from fuel to air side [25]. This behavior could be an important drawback for SOFCs working at temperatures around 550-600 °C, as it has been demonstrated that AISI 441 exposed to dual atmosphere at 600 °C suffered severe **breakaway corrosion** [26]. Different explanations have been proposed, e.g. that hydrogen would increase internal oxidation reducing chromium supply and so cause breakaway corrosion, but no theory is universally accepted for the moment. Most of the cited studies used uncoated substrates, to accelerate the degradation kinetics and uncouple the influence of a coating.

Mechanical stress

FSS's have been chosen as interconnect material among others because of their good CTE compatibility with the ceramic components in a SOFC stack. Still the difference in lattice parameters between steel substrate, thermally grown oxide and protective coating causes residual mechanical stresses during heating / cooling of the stack and can lead to spallation of the scale or the protective layer. During heating and scale growth the scale is subjected to tensile stresses because of the higher thermal expansion of the steel compared to that of the scale. Conversely, compression stresses in the scale arise during cooling. Understanding of the thermal stresses in the stack components is of high relevance to meet the reliability requirements of SOFC systems. In addition, due to the increasing interest to fit the SOFC systems operation to the user power demand, SOFC stacks have to withstand **thermal cycling** during their lifetime. Thermal cycling exposes the stack components to faster mechanical degradation, caused not only by the mismatch of thermal expansion between the materials but also by thermal gradients during heat up/cool down. In literature there is convergence to use the Griffith fracture approach: a certain energy (given by shear stress in this case) threshold must be overcome in order to cause failure of the ceramic materials.

The interfacial strength is measured experimentally using either an indentation test (e.g. Rockwell) or a 4-pt bending test. Knowing the other mechanical properties of the materials studied, it is possible to correlate this value to a certain oxide layer thickness, which in turn, coupled with a kinetic curve for oxide layer growth, could **forecast the adhesion lifetime** of the ceramic layers (oxide layer or protective coating). As an example, Liu et al. forecasted the lifetime of coated (with $MnCo_2O_4$) and uncoated Crofer 22 APU substrates [27]. The samples are first oxidized at 800 °C and then cooled to room temperature to simulate the stress due to a turning off of the system. Then, a Rockwell indentation test is performed. From these test results, they found the strength at the interface (both at metal/scale and at scale/coating) which is the maximum shear stress tolerated by the samples. The experimental data were then used in a FEM model to obtain the interfacial strength as a function of the scale thickness. The model predicts a lifetime of about 4800 h for uncoated Crofer 22 APU and 15000 h when coated with $MnCo_2O_4$. These results reflect a critical scale thickness of 11.4 µm and 4.2 µm respectively.

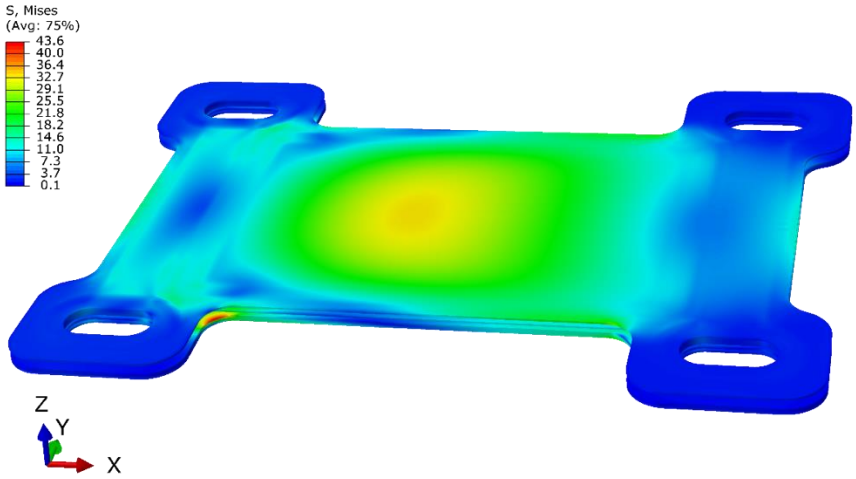

Figure 2. Plot of the Von Mises stress field at high temperature in a SOLIDpower MIC cassette. The stress field is calculated by FEA simulating the stack production process steps, followed by co-flow operation. Operating conditions used to generate the simulated temperature profile are $T_{fuel,in}$ = 700 °C, $T_{air,in}$ = 700 °C, prereforming 50%, FU = 0.85 and $T_{max,cell}$ = 827 °C. Regions with high stresses indicate possible plastic deformation as well as risk of buckling.

Models like the aforementioned one estimate stress inside the MIC with finite element simulations. Figure 2 shows an example. A temperature profile was imported into a FEA model obtained from combined thermo-electrochemical and fluid dynamics models. Figure 2 depicts the Von Mises stresses in the metallic interconnect of an SOFC stack model simulated in co-flow configuration. The center of the MIC cassette is exposed to the highest temperatures, because of the electrochemical reactions occurring at the cell. Considering that stresses in SOFC stacks are generated, among others, by thermal gradients and thermal expansion mismatch between the components, the highest Von Mises stresses in the IC are located at the central area of the cassette, shown in Figure 2. The IC might buckle in this area, especially if it is relatively thin. In turn, **buckling** may provoke i) on one face, damage of the adjacent elements, i.e. inelastic deformation of the GDLs and ii) detachment of the interface, on the opposite face. As a result, stack reliability is affected also by the stresses in the IC. To investigate thermo-mechanical reliability of SOFC stacks upon operation, scenarios of long-term operation, thermal cycling, and a combination of them have been simulated [34]. Using the stress states simulated by the FEA model, mechanical reliability analysis of SOFC stacks was then carried out either by applying fracture mechanics or by investigation of the contact pressure between the stack components. Contact pressure influences the electrical current pathways between IC and cell and thus the stack performance and durability [28][29].

Nonetheless, thermo-mechanical degradation of interconnects in real stacks appears to be less dramatic than predicted by modeling: in a stack run for 35000h and containing Fe-doped $MnCo_2O_4$ (MCF) coated Crofer 22 APU interconnects (same steel substrate as in [27]), no sign of delamination at the steel/scale or scale/MCF interface occurred, even though the average scale thickness was between 3-5 μm [30] and the model of Liu et al. predicted delamination at 4.2 μm scale thickness for coated surfaces.

7.3 Solutions to decrease IC degradation

Tuning the alloy composition is one strategy adopted to mitigate MIC degradation. Reactive elements addition in the alloy affects the oxygen and chromium diffusion coefficients in thermally grown Cr_2O_3, decreasing its kinetic growth [31, 32]. The addition of reactive elements (e.g. small amounts of Ce, La or Y) improves as well the scale adhesion to the alloy substrate and therefore the resistance to thermal cycling. Another important alloying element is Mn. Its fast diffusion across the chromia scale [16] and interaction with

chromium leads to the formation of a preferred $(Cr,Mn)_3O_4$ spinel phase at the gas interface of the thermally grown oxide scales. This spinel phase positively influences the electrical conductivity [2] and in addition reduces the undesirable Cr evaporation.

Alloy composition alone is not sufficient to achieve the desired IC lifetime. The deposition of protective coatings on the alloy surface has been established as a *sine qua non* for long term SOFC application. Spinel and perovskite coatings are commonly used. Their deposition techniques play an important role, as they lead to different microstructures, in particular the coating density. The effectiveness of a protective coating in improving the electrical contact is evident when comparing ASR results for coated and uncoated alloys substrates. The difference may be one order of magnitude, and a similar result is found for the same coating on top of different steels. With the coating material being equal, high coating density deposition methods like PVD or atmospheric plasma spray (APS) give better results. Figure 3 illustrates the microstructures that help explain such results. Figure 3*a* shows a $MnCo_2O_4$ protective coating deposited by wet powder spray which remains porous, leading to a thicker Cr_2O_3 scale grown on top of the FSS substrate, with respect to APS and PVD deposited dense coatings, in Figure 3*b* and Figure 3*c*, respectively. PVD coatings on FSS lead to the lowest contact resistance, thus represent the state-of-the-art [11, 33].

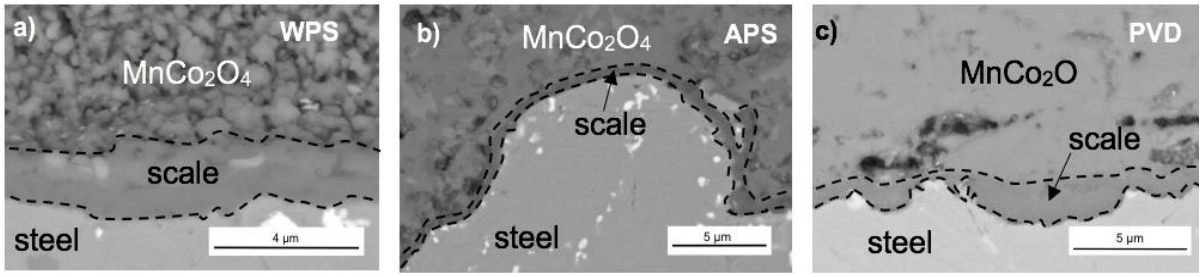

Figure 3. Thermal oxide grown on FSS substrates coated with different coating techniques but same protective layer ($MnCo_2O_4$): a) wet powder spray, b) atmospheric plasma spray c) physical vapour deposition. High density coatings lead to the best results in terms of minimum scale thickness, which in turn gives lower contact resistive loss for samples b) and c)

Cr retention properties of spinels are depicted in Figure 4. In this case too, the denser coatings like PVD and APS show the best performances. The dense spinels protected a 200 µm $La_{1-x}Sr_xCoO_3$ (LSC) cathode from Cr poisoning for 1000 h at 700 °C (Figure 4b) while the one deposited with WPS let chromium poison the LSC cathode, producing the low electrically conductive phase $SrCrO_4$ (white dense layer at coating-cathode interface in Figure 4a).

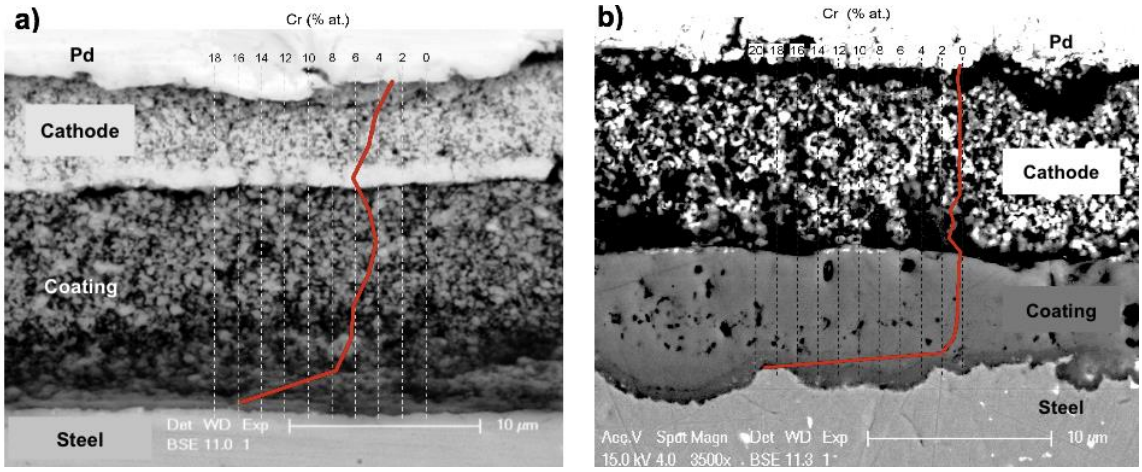

Figure 4. LSC cathode material in contact with FSS substrate coated by MCO spinel: Cr diffusion profile expressed in atomic percentage. a) MCO deposited via WPS: Cr poisoning of the LSC, b) MCO deposited via PVD: excellent Cr retention. Pd is a counter contact plate in the ASR test set-up.

The effectiveness of coatings has been demonstrated in the long term on stacks (Table 2). Currently the main drawbacks of these coatings and their deposition techniques are the associated production cost and the environmental impact, Co being a hazardous and critical element [34].

From the mechanical point of view, the poor creep resistance of ferritic stainless steels is improved with the addition of Nb and/or W. These elements lead to Laves phases, intermetallic compounds with the composition AB_2 (e.g. Fe_2Nb), which segregate at the grain boundaries and induce precipitation hardening [35]. Crofer 22H (cfr. Table 1) segregates Nb-W containing precipitates at the grain boundaries - Crofer 22APU with similar composition to Crofer H but without Nb and W, shows no sign of these phases. The precise correlation between Laves phase precipitation and creep strengthening has not been found yet, as other precipitates strengthen the FFS microstructure too. In addition, Ostwald ripening of Laves phases can decrease the mechanical properties of the material leading to a ductile-to-brittle transition. Coarsening of the Laves phases must be delayed to ensure long life of the interconnect [36]. Laves phases segregate below the scale too (Fig 5); this, together with their affinity for Si, may be a cause of interconnect electrical behavior degradation [32].

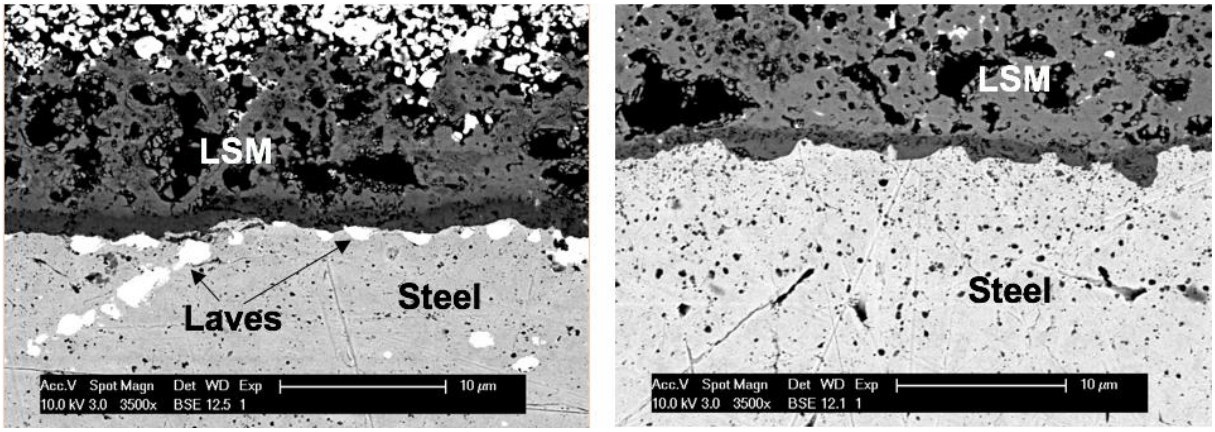

Figure 5. Comparison of steel/scale interface for Crofer 22H (left) and APU (right). Steels aged for 3000h @ 800 °C in air and current density of 0.35 Acm^{-2}. Laves phases accumulation below the scale in Crofer 22H is clearly visible.

7.4 Degradation of stacks and cells

Table 2 summarizes long term results on present S-o-A stacks, with a focus on the observed MIC degradation phenomena.

Ref.	*MIC alloy & coating*	*Testing conditions*	*Cell*	*Stack degradation*	*Interconnect behavior*
			Anode supported		
1 **[37]**	Crofer 22APU Mn_2O_3 (WPS)	~17000 h 700 °C 0.5 A/cm^2	*Anode*:Ni-YSZ (H_2/3%H_2O) *Cathode*: LSCF (air)	10 mV/kh < 4 kh 17.5 mV/kh > 4 kh	Mn_2O_3 lets Cr migrate → $SrCrO_4$ grown on LSCF → progressive stack degradation @ cathode side: 4 μm scale thickness; local Cr_2O_3 breakaway with Fe-oxide spots (but no short-circuits between MICs). @ anode side: 2 μm scale thickness; Ni diffusion into Crofer 22APU → austenite phase creation
2 **[38]**	Crofer 22APU MCF (APS)	~ 19000 h 800 °C 0.5 A/cm^2	*Anode*: Ni-YSZ (H_2/3%H_2O) *Cathode:* LSM (air)	4 mV/kh	small cracks in MCF but no delamination thicker scale at the uncoated anode side (12 μm) than at the coated cathode side (3 μm) micropores accumulation in the MCF at the MIC/MCF interface humidity present at anode side leads to porosity in the anode side scale (11-12 μm thick)
3 **[29]**	Crofer 22APU MCF (APS)	~35000 h 700 °C 0.5 A/cm^2	*Anode:* Ni-YSZ H_2/25%H_2O *Cathode:* LSCF(air)	0.3%/kh	@cathode side: 3-5 μm thick Cr-Mn scale. No spallation at the steel/scale/MCF interface. No Cr diffusion into LSCF @ anode side: Ni diffusion (from contacting wires) lead to a 50-100 μm wide austenized zone. No brittle σ-phase precipitates were found in the same area. no enhanced corrosion at the steel/sealing interface
4 **[39]**	Crofer 22APU MCF (APS)	~6000 h 700 °C 0.5 A/cm^2	Anode: Ni-YSZ (LNG 7.2 slm, H_2 3.2 slm, H_2O 15.2 slm) *Cathode*: LSCF (air)	0.3%/kh for 4.5 kh	strong MCF adhesion on Crofer 22 APU no cracks penetrating through the coating MCF coating retained chromium melting of IC and sealing glass occurred in one cell because of a leakage in the sealant
5 (SP)	AISI 441 MCO (WPS)	~5000h 780 °C 0.4 A/cm^2	*Anode:* Ni-YSZ (N_2/H_2) *Cathode*:LSC (air)	0.4%/kh	@ cathode side: thicker scale on the IC ribs (~5 μm) wrt to the valleys (~3 μm). Fe diffuses through Cr_2O_3 and Cr diffuses through MCO. good adherence: no coating or scale spallation densification of the MCO coating where the ribs are in contact with LSC. A possible reason is Fe diffusion into MCO from the steel substrate no enhanced corrosion due to dual atmosphere @anode side: no coating, yet corrosion was not aggressive (~ 5 μm)
6 (SP)	AISI 441 Spinel (WPS)	2600h 760 °C 124 thermal cycles	*Anode:* Ni-YSZ(N_2/H_2) *Cathode*:LSC(air)	-	@cathode side: scale thickness < 3μm where MIC not in contact with the cathode (rib), ca. 10μm where the MIC was in contact with the cathode (valley). Fe breakaway corrosion into the scale and the spinel coating no sign of delamination at the steel/scale and scale/protective coating interface despite the 124 thermal cycles
	IC alloy	*Testing Conditions*	*Cell*	*Stack degradation*	*Interconnect behavior*

	& Coating				
7 **[40]**	AISI 441 Ce-MCO (Slurry) on LSM // Al_2O_3 where there is sealing	6000 h 800 °C 0.3 A/cm^2	*Anode*: Ni-YSZ (H_2,N_2(1:1) + 3% H_2O) *Cathode:*LSM-YSZ(air)	~1.4%/kh	@ AISI441/Ni-current collector interface corrosion is enhanced if Ni wires' diameter <100 μm @ cathode side: Cr depletion below the scale (16%at. instead of 20%at.) No Cr traces in LSM. No spallation at scale/IC interface Si, Ti accumulation below the scale, but no continuous layer
			Electrolyte supported		
8 **[17][41]**	CFY LSM(-)	~40000 h 900 °C 0.25 A/cm^2	*Anode:*Ni/CGO (CPO + reformed natural gas) *Cathode*:LSM(air)	-	Considering the IC ribs geometry, faster scale grows at the IC/cathode interface than in the IC valley. This happens for both cathode and anode. Higher average scale thickness at anode with respect to cathode Different CFY behavior at anode side: @ the inlet valley, Cr_2N compound is found @ the center, the interaction of the oxide layer with the Ni-mesh is more intense; @ the outlet valley, more pores in scale compared to the scale under the ribs MIC-cell thermal mismatch lead to local stress peaks which in turn boost crack propagation
			Metal supported		
9 **[42]**	FeCr alloy powders	1100 h 650 °C 0.25 A/cm^2	*Anode*: CGO-Ni (H_2/3%H_2O) *Cathode*: LSCF/CGO	(single cell) ~5%/kh	Increment in ohmic losses due to corrosion interlayer in between metal substrate and infiltrated CGO
10 **[43]**	FeCr powders Ni-CGO	500 h 850 °C	*Anode:*STN/FeCr (pH_2O/pH_2=9) Half-cell	-	STN:FeCr half-cell showed better corrosion resistance than reference YSZ:FeCr reference cell STN:FeCr (50:50) composition demonstrated a better oxidation resistance than STN:FeCr (70:30) (Corrosion test done on half cells composed of FeCr/ STN:FeCr infiltrated by Ni-CGO)

Table 2. Long-term tests of stacks or cells based on different structural technology

7.5. Summary

Metal interconnect corrosion causes an increase in stack ohmic resistance, while mechanical stress may trigger structural rupture and failures in electrical contacts. The influence of air/fuel environment (pO_2, pH_2, pH_2O) on the FSS ageing process is not completely understood yet, even if there is a tendency to consider the corrosion process independent of pO_2 and accelerated by pH_2O. Separate experiments showed higher degradation kinetics of uncoated FSS in dual atmosphere condition, but observations on MICs tested in commercial-like stacks (=dual atmosphere) did not show any dramatic corrosion.
SOFC-customized steel composition and protective coatings have been developed to ensure the goal of >40000 h stack life. An overview of the solutions was given, with the conclusion that high density coating techniques such as PVD or APS are the options leading to best performance.
A table summarized results of stacks with different cell types tested in operating conditions for medium to extended durations. The post-test analysis of these stacks/cells indicate that the materials appear more resistant to ageing than expected from simulation and separate tests performed in out-of-stack conditions. This illustrates on the one hand that models can overestimate the materials degradation, and on the other hand that current solutions to extend lifetime are already reasonably effective.

7.6. Bibliography metal interconnects

[1] F. Tietz, *Ionics*, Vol. 5(1), 1999, pp. 129-139
[2] W.Z. Zhu, S. C. Deevi, *Mater. Sci. Eng. A*, 348(1-2), 2003, pp. 227-243
[3] H. Yokokawa, *Perovskite Oxide for Solid Oxide Fuel Cells* (ed. 2009), Chapter 2, Springer
[4] J. Wu, Xingbo Liu, *J. Mater. Sci. Technol.*, 26(4), 2010, pp. 293-305
[5] M. R. Terner, J. Andreas Schuler, Andreas Mai, Dirk Penner, *Solid State Ionics*, 263, 2014, pp. 180-189
[6] J. Pappis, W. D. Kingery, *J. Am. Ceram. Soc.*, 44(9), 1961, pp. 459-464
[7] M. Stanislowski, E. Wessel, K. Hilpert, T. Markus, L. Singheiser, *J. Electrochem. Soc.*, 154(4), 2007, pp. A295-A306
[8] Z. Yang, K. S. Weil, D. M. Paxton, J. W. Stevenson, *J. Electrochem. Soc.*, 150(9), 2003, pp. A1188-A1201
[9] Plansee, CFY factsheet, https://www.plansee.com/en/materials/chromium.html, last visit 12.2016.
[10] J. Tallgren, M. Bianco, J. Mikkola, O. Himanen, M. Rautanen, J. Kiviaho, J. Van herle, *XII EFCF Proceedings*, 2016, B06, pp. 114-124
[11] VDM Metals, Crofer 22 APU datasheet, http://www.vdm-metals.com/fileadmin/user_upload/Downloads/Data_Sheets/Data_Sheet_VDM_Crofer_22_APU.pdf, last visit 12.2016.
[12] M. Stanislowski, J. Froitzheim, L. Niewolak, W.J. Quadakkers, K. Hilpert, T. Markus, L. Singheiser, *J. Power Sources*, 164, 2007, pp. 578-589
[13] L. L. Shreir, *Corrosion* (ed. 1994), Chapter 1, Butterworth-Heinemann
[14] C. Wagner, *J. Electrochem. Soc.*, 99(10), 1952, pp. 369-380
[15] Tomasz Brylewski, Makoto Tanko, Toshio Maruyama, Kazimierz Przybylski, *Solid State Ionics*, 143(2), 2001, 131–150
[16] M. Palcut, L. Mikkelsen, K. Neufeld, M. Chen, R. Knibbe, P. V. Hendriksen, *Corrosion Science*, 52(10), 2010, 3309-3320
[17] M. Linder, T. Hocker, L. Holzer, K. Friedrich, B. Iwanschitz, A. Mai, J. A. Schuler, *J. Power Sources*, 243, 2013, 508-518
[18] S. Fontana, S. Chevalier, G. Caboche, *Oxid. of Met.*, 78(5), pp. 307-328
[19] M. Linder, T. Hocker, L. Holzer, K. Friedrich, B. Iwanschitz, A. Mai, J. A. Schuler, *J. Power Sources*, 272, 2014, 595-605
[20] H. Nagai, S. Ishikawa, N. Amano, K. Shoji, *Transactions of the Japan Institute of Metals*, 26(10), 1985, pp. 753-762
[21] M.Linder, T. Hocker, L. Holzer, O. Pecho, K. A. Friedrich, T. Morawietz, R. Hiesgen, R. Kontic, B. Iwanschitz, A. Mai, J. A. Schuler, *Solid State Ionics*, 283, 2015, pp. 38-51
[22] E. A. Polman, T. Fransen, P. J. Gellings, *J. Phys.: Condens. Matter*, 1(28), 1989, pp 4497-4510
[23] P. Alnegren, M. Sattari, J. Froitzheim, J-E. Svensson, *Corrosion Science*, 110, 2016, pp. 200-212
[24] S.R.J. Saunders, M. Monteiro, F. Rizzo, *Progress in Materials Science,* 53(5), 2008, pp. 775–837
[25] Zhenguo Yang, Guanguang Xia, Prabhakar Singh, Jeffry W. Stevenson, *Solid State Ionic*s, 176(17-18), 2005,1495-1503
[26] P. Alnegren, M. Sattari, J. Svensson, J. Froitzheim, *J. Power Sources*, 301, 2016, pp. 170-178
[27] W.N. Liu, X. Sun, E. Stephens, M.A. Khaleel, *J. Power Sources*, 189(2), 2009, pp. 1044-1050
[28] F. Greco, A. Nakajo, Z. Wuillelmin, J. Van herle, *ECS transaction*, 68(1), 2015, pp. 1921-1931
[29] A. Nakajo, Z. Wuillemin, J. Van herle, D. Favrat, *J. Power Sources*, 193(1), 2009, pp. 216-226
[30] N. H. Menzler, P. Batfalsky, A. Beez, L. Blum, S. Gross-Barsnick, L. Niewolak, W. J. Quaddakers, R. Vassen, *XII EFCF Proceedings*, 2016, A11, pp. 290-297
[31] E. Lang, *The role of active elements in the oxidation behaviour of high temperature metals and alloys* (ed. 1989), Elsevier.
[32] S. Chevalier, *Materials and Corrosion*, 65(2), 2014, pp. 109-113
[33] M. Bianco, M. Auchlin, S. Diethelm, J. Van herle, *XII EFCF Proceedings, 2016,* B05, pp. 98-107
[34] *Report on critical raw materials for the EU*, 2014

[35] J. Froitzheim, G.H. Meier, L. Niewolak, P.J. Ennis, H. Hattendorf, L. Singheiser, W.J. Quadakkers, *J. Power Sources*, 178(1), 2008, pp. 163-173
[36] S. Zhu, M. Yang, X.L. Song, S. Tang, Z.D. Xiang, *Mat. Charac.*, 98, 2014, pp. 60-65
[37] N.H. Menzler, P. Batfalsky, S. Groß, V. Shemet, F. Tietz, *ECS transaction*, 35(1), 2011, pp. 195-206
[38] J. Malzbender, P. Batfalsky, R. Vaßen, V. Shemet, F. Tietz, *J. Power Sources*, 201, 2012, pp. 196-203
[39] Q. Fang, L. Blum, P. Batfalsky, N. Menzler, U. Packbier, D. Stolten, *Int. J. Hydrogen Energy*,38(36),2013,16344-16353
[40] Y.-S. Chou, J. W. Stevenson, J.-P. Choi, *J. Power Sources*, 257, 2014, pp. 444-453
[41] F. Fleischhauer, A. Tiefenauer, T. Graule, R. Danzer, A. Mai, J. Kuebler, *J. Power Sources*, 258, 2014, pp. 382-390
[42] P. Blennow, J. Hjelm, T. Klemensø, S. Ramousse, A. Kromp, A. Leonide, A. Weber, *J. Power sources*, 196(17), 2011, pp. 7117-7125
[43] P. Blennow, A. H. Persson, J. Nielsen, B. R. Sudireddy, T. Klemenso, *X EFCF Proceedings*, 2012, A09, pp. 72-83

8. Priorisation of degradation for INSIGHT – process by process

Based on the present knowledge and literature review as summarised above, and on test & field experience of the understanding, identification, detection and mitigation/ recovery potential of the various SOFC stack degradation processes, they are discussed in the following one by one.

A table of identical structure for every process is given:

1. underlying cause of the process (physicochemical, mechanical,..)
2. influencing parameters (T, p,…)
3. effect of the cause (voltage –drop etc.)
4. whether the process can cause the End-of-Life (EOL) of a stack (yes/no)
5. whether the process can be avoided
6. whether it can be recovered and how
7. how it could be detected (among others refering to Table 3 with the identified EIS frequency range)
8. which parameters might accelerate it
9. how 'on purpose faults' could be introduced to investigate specifically the process in question.

Each process is then marked with an evaluation by each Task-contributing partner (EPFL, CEA, DTU, HTc/SP), with a severity mark (1 = mild, 2 = medium 3 = severe) times an occurrence mark (1 = rare, 2 = regular, 3 = frequent) to give a risk number (between 1 x 1 = 1 (minimal risk) and 3 x 3 = 9 (maximal risk)). In addition, each partner also indicates a qualitative mark to each process (A = high priority – B = medium priority – C = low priority).

In the end, all evaluation results are synthesized and compared.
This should lead to a proposed classification for the priority processes to consider for the INSIGHT project.

Anode1	Ni coarsening
Cause	surface energy minimisation
Parameters	T, pH_2O, initial microstructure
Effect	TPBL ↓, V ↓
EOL	no
Avoidance	none
Recovery	current treatment
Detection	P5, P2, R_Ω
Acceleration	T, pH_2O
On purpose faults	nano-NiO starting powder?

Survey results :

	EPFL	CEA	DTU	HTc/SP	Avg
Severity	**1**	**1**	**1**	**1**	**1**
x Occurrence probability	**3**	**3**	**3**	**3**	**3**
= Risk	**3**	**3**	**3**	**3**	**3**
Qualitative mark	**C**	**B ?**	**A ?**	**C**	**C**

Remarks:
Common evaluation by all partners.
Quality marks 'B' and 'A' by CEA and DTU seem not sure, given the low risk marks (3) that were attributed.

Anode2	Ni reoxidation
Cause	Ni – NiO – (p, T) equilibrium
Parameters	high FU, starvation, seal leakage, gas supply issue
Effect	V ↓ anode and or electrolyte cracking
EOL	yes
Avoidance	flow field design, redox-robust anode
Recovery	lower UF, or OCV operation; current treatment?
Detection	P5, P2, R_Ω
Acceleration	low fuel flow
On purpose faults	stop fuel flow

Survey results :

	EPFL	CEA	DTU	HTc/SP	Avg
Severity	**3**	**3**	**3**	**3**	**3**
x Occurrence probability	**2**	**2**	**1**	**1**	**1.5**
= Risk	**6**	**6**	**3**	**3**	**4.5**
Qualitative mark	**A**	**A**	**B** should not occur under normal operation	**A?** typically avoided but harmful	**A**

Remarks:
Consensus on maximal 'severity'.
Not clear whether mark 'A' was meant by HTc/SP, for a relatively low risk (3). Nonetheless an overall grade of 'A' is attributed to this process.

Anode3	Carbon deposition
Cause	Thermodynamics of C-H-O as f(T, p) and fast kinetics > 500°C
Parameters	O/C ratio, T
Effect	C adsorption on Ni, Ni encapsulation, anode pore blocking, fuel channel blocking, reformer clogging
EOL	yes
Avoidance	Ensure sufficient O/C ratio, water supply
Recovery	steam/CO_2 flush, j↑(electrochemical oxidation), increase H_2 content
Detection	Δp(anode, reformer), reformer-T, λ-sensor before and after reformer, P2, P5 R_Ω ↓!
Acceleration	reduce water supply
On purpose faults	insufficient O/C

Survey results :

	EPFL	CEA	DTU	HTc/SP	Avg
Severity	**3**	**3**	**3**	**3**	**3**
x Occurrence probability	**2**	**2**	**1**	**1**	**1.5**
= Risk	**6**	**6**	**3**	**3**	**4.5**
Qualitative mark	**A**	**B**	**A?** should not occur under normal operation	**A?** typically voided but harmful	**A**

Remarks:
Consensus on maximal severity (3).
Mixed evaluation on likelihood.
Not clear whether mark 'A' was meant by DTU and HTc/SP, for a relatively low risk (3). Nonetheless an overall grade of 'A' is attributed to this process..

Anode4	S-poisoning , other poisoning (Si, Cl, …)
Cause	Ni-S adsorption equilibrium as fct(T, pS)
Parameters	S-concentration ↑T ↓C-fuel more severe than H_2
Effect	rapid V-drop ↓reforming and WGS reactons hindered
EOL	no (only in severe cases)
Avoidance	S-trap
Recovery	stop S-flow; T↑ H_2-operation
Detection	S-detector at trap outlet P5, P2
Acceleration	high S-concentration
On purpose faults	bypass S-trap

Survey results :

	EPFL	CEA	DTU	HTc/SP	Avg
Severity	**2**	**1**	**3**	**1**	**1.75**
x Occurrence probability	**1**	**3**	**2**	**3**	**2.25**
= Risk	**2**	**3**	**6**	**3**	**3.94**
Qualitative mark	**C**	**B**	**B** Should not occur under normal operation	**B**	**B**

Remarks:
Very mixed evaluation in both severity and frequency. Nonetheless regarded as a process of medium priority (B) since avoidance and recovery measures exist.

Cathode1	2nd phase formation ($SrZrO_3$)
Cause	Sr activity and mobility
Parameters	high T_{sinter}, high T_{op}, pH_2O, CGO porosity
Effect	potential current constriction at CGO-YSZ interface Sr loss => cathode deactivation (R_{pol})
EOL	no
Avoidance	dense CGO ; this does not avoid cathode decomposition however
Recovery	none
Detection	R_Ω ? P3?
Acceleration	air humidity
On purpose faults	age in SOEC conditions (SrZrO3 formation is more severe), then test in SOFC mode

Survey results :

	EPFL	CEA	DTU	HTc/SP	Avg
Severity	**1**	**1**	**2**	**1**	**1.25**
x Occurrence probability	**2**	**3**	**1**	**3**	**2.25**
= Risk	**2**	**3**	**2**	**3**	**2.81**
Qualitative Mark	**C**	**B**	C	**C** question if this is problematic, as conduction through ceria in barrier layer is not compromised	**C**

Remarks:
Whereas the process is known to occur, it is regarded of relativily low priority since also it is unlikely recoverable.

Cathode2	LSCF decomposition (incl. Cr-poisoning)
Cause	Sr activity & mobility; Fe loss; Co loss
Parameters	high T, pH_2O, Sr-getters (Cr => $SrCrO_4$, S => $SrSO_4$, Si => La-Sr-silicate, CO_2 => $SrCO_3$)
Effect	R_{pol} ↑ V ↓ reduced porosity
EOL	?
Avoidance	change cathode composition; no leakage (air humidity); no other contamination (CO_2, Cr, S, Si,..)
Recovery	T_{op} ↑ ? operation at η_{cath} ↑ or η_{an} ↑? (this is controversial in literature) operation at reduced pO_2 (e.g. 5%, not 21%)?
Detection	P3 (R_{pol}), P1 (O_2-dissoc), (R_Ω), P2 (when reduced porosity)
Acceleration	pH_2O, pCO_2 at air side
On purpose faults	high air humidity

Survey results :

	EPFL	CEA	DTU	HTc/SP	Avg
Severity	**2**	**1**	**2**	**1**	**1.5**
x Occurrence probability	**3**	**3**	**1**	**3**	**2.5**
= Risk	**6**	**3**	**2**	**3**	**3.75**
Qualitative Mark	**A**	**B**	**C**	**C** unavoidable but not too problematic	**B**

Remarks:
Relative consensus on a process of medium priority in SOFC operation.

MIC1	Contact loss (deformation, creep)
Cause	thermomechanical properties & stress, Δ–TEC
Parameters	T-cycling ; loadcycling (j)
Effect	spallation, delamination, V ↓ channel blocking (when deformation)
EOL	no (only in most severe cases)
Avoidance	MIC choice and assembly quality
Recovery	Increase compression? T ↑?
Detection	RΩ ↕ (P2), Δp cathode?
Acceleration	T-cycling
On purpose faults	introduce a bad contact

Survey results :

	EPFL	CEA	DTU	HTc/SP	Avg
Severity	**3**	**3**	**3**	**3**	**3**
x Occurrence probability	**2**	**1**	**2**	**1**	**1.5**
= Risk	**6**	**3**	**6**	**3**	**4.5**
Qualitative mark	**B**	**B**	**A**	**B**	**B**

Remarks:
Consensus on maximal severity of this process, with an average risk and priority attribution.

MIC2	Corrosion
Cause	oxidation of Cr, Si,.. alloying elements
Parameters	T ↑ pO_2, pH_2O ↑
Effect	scale formation; electrode poisoning (Cr, Si) ; V ↓
EOL	no
Avoidance	MIC choice; protective coating choice, and sufficiently dense coating; no air humidity
Recovery	Cr revolatilisation? (OCV or reverse polarity operation)
Detection	R_Ω ↑(scale); P3 (Cr poisoning); P2 (cathode pore blocking)
Acceleration	T ↑ pH_2O ↑
On purpose faults	no protective layer

Survey results :

	EPFL	CEA	DTU	HTc/SP	Avg
Severity	**2**	**1**	**3**	**1**	**1.75**
x Occurrence probability	**3**	**3**	**1**	**3**	**2.5**
= Risk	**6**	**3**	**3**	**3**	**4.375**
Qualitative mark	**B**	**C**	**B** should be avoided by protective coatings	**C** corrosion unavoidable, Cr will volatilize but does not harm the cathode	**B/C**

Remarks:
Process known to occur anyway, but regarded as unrecoverable and with limited / avoidable effect (protective coating).

Seal1	Mechanical failure (leakage)
Cause	thermomechanical properties, Δ–CTE
Parameters	T-cycling, $\Delta P_{an\text{-}cath}$ ↑
Effect	V ↓, hot spot, gas mixing, (fuel) efficiency loss
EOL	yes
Avoidance	minimize Δ–CTE, minimize $\Delta P_{an\text{-}cath}$, ensure constant compression
Recovery	compression ↑? self-healing by T ↑?
Detection	OCV ↓, T ↑, air humidity, λ-sensor, $\Delta P_{an\text{-}cath}$, ΔP_{an}, ΔP_{cath}
Acceleration	high $\Delta P_{an\text{-}cath}$
On purpose faults	seal with opening

Survey results :

	EPFL	CEA	DTU	HTc/SP	Avg
Severity	**3**	**2**	**2**	**2**	**2.25**
x Occurrence probability	**2**	**2**	**2**	**2**	**2**
= Risk	**6**	**4**	**4**	**4**	**4.5**
Qualitative mark	**A**	**A**	**A** input from field tests needed	**A**	**A**

Remarks:
Consensus on a priority process.

Seal2	Volatility, reactivity (+decomposition)
Cause	thdyn driving force to react with materials in contact; high P_{evap} (of seal elements, e.g. B)
Parameters	T
Effect	seal porosity, $BaCrO_4$ formation, electrode poisoning
EOL	no
Avoidance	seal composition; no contact with reactive materials
Recovery	self-healing by T ↑?
Detection	OCV ↓ T ↑ air humidity, λ-sensor, $\Delta P_{an\text{-}cath}$, ΔP_{an}, ΔP_{cath}, P3 (cathode poisoning), P5 (anode poisoning), P2
Acceleration	high T
On purpose faults	use a more reactive/volatile sealing material

Survey results :

	EPFL	CEA	DTU	HTc/SP	Avg
Severity	**3**	**3**	**2**	**1**	**2.25**
x Occurrence probability	**1**	**1**	**2**	**2**	**1.5**
= Risk	**3**	**3**	**4**	**2**	**3.375**
Qualitative mark	**C**	**B**	**C** Input from field tests needed	**B**	**B/C**

Remarks:
Mixed evaluation for a process of average risk and priority.

Ely1	Cracks, embrittlement
Cause	thermomechanical properties; CGO fabrication
Parameters	T-cycling, leakages (=> e.g. Ni reoxidation cracking the YSZ)
Effect	V ↓ hot spot, gas mixing
EOL	yes
Avoidance	Redox-robust anode, Δ–TEC match
Recovery	(self-healing – exceptional)
Detection	OCV ↓ T ↑ air humidity, λ-sensor, $\Delta P_{an\text{-}cath}$, P2, R_{Ω}, P5, P3
Acceleration	?
On purpose faults	test rejected (out-of-spec) cells (e.g. with pinholes or small cracks)

Survey results :

	EPFL	CEA	DTU	HTc/SP	Avg
Severity	3	3	3	3	3
x Occurrence probability	1	1	1	1	1
= Risk	3	3	3	3	3
Qualitative mark	C	C	C	C goes hand in hand with anode reoxidation	C

Remarks:
Strong overall consensus on severe but normally rare process, hence of low priority, also because it's irreversible.

Ely2	Reactivity, porosity (CGO), conductivity
Cause	driving force YSZ-CGO reaction; CGO fabrication; vacancy ordering
Parameters	T_{sinter} ↑
Effect	increased R_{Ω}-drop, $SrZrO_3$ formation
EOL	no
Avoidance	dense CGO; low T_{sinter}
Recovery	none
Detection	R_{Ω} ↑
Acceleration	T ↑
On purpose faults	very porous CGO

Survey results :

	EPFL	CEA	DTU	HTc/SP	Avg
Severity	**1**	**1**	**2**	**1**	**1.25**
x Occurrence probability	**3**	**3**	**1**	**1**	**2**
= Risk	**3**	**3**	**2**	**1**	**2.5**
Qualitative mark	**C**	**B**	**C**	**C** very long term	**C**

Remarks:
Regarded as a low priority process.

A Summary table of all degradation phenomena survey, grouping the most relevant information and survey marks, is given on the next page, with the reminder of the detectable processes.

Component	Process	Sev.	Freq.	Risk	Recovery	Detection	Σ
Anode	Coarsening	1	3	3	Current treatment	P5, P2, R_Ω	**C**
	Reoxidation	3	1.5	4.5	lower UF, **OCV operation; current treatment**	**P5,** P2, R_Ω	**A**
	C deposition	3	1.5	4.5	**steam/CO_2 flush**, j ↑ (electrochemical oxidation), increase H_2	**Δp(anode, reformer), reformer-T, λ-sensors (O/C-ratio),** P2, P5, R_Ω ↓	**A**
	S poisoning	1.75	2.25	3.94	stop S-flow; T ↑ H_2-operation	S-detector at trap outlet; P5, P2	**B**
Cathode	$SrZrO_3$ formation	1.25	2.25	2.81	none	R_Ω ?, P3?	**C**
	Demixing	1.5	2.5	3.75	T_{op} ↑ ? η_{cath} ↑ or η_{an} ? (controversial); operation at **reduced pO_2 (e.g.5%)?**	**P3** (R_{pol}), **P1** (O_2-dissoc), (R_Ω), P2 (when reduced porosity)	**B**
MIC	Contact loss	3	1.5	4.5	Compression? T ↑?	R_Ω, (P2), Δp cathode?	**B**
	Corrosion + poisoning	1.75	2.5	4.38	Cr revolatilisation? (OCV or reverse polarity?)	R_Ω (scale); P3 (Cr poisoning); P2 (cathode pore blocking)	**B/C**
Sealing	Leakage	2.25	2	4.5	**compression** ↑? **self-healing** by T ↑?	**OCV** ↓ **T** ↑ **cathode outlet humidity**, λ-sensor **$\Delta P_{an\text{-}cath}$**, ΔP_{an}, ΔP_{cath}	**A**
	Reactivity + Poisoning	2.25	1.5	3.38	self-healing by T ↑?	OCV ↓ T ↑ air humidity, λ-sensor, $\Delta P_{an\text{-}cath}$, ΔP_{an}, ΔP_{cath}, P3/P5 (poisoning), P2	**B/C**
Electrolyte	Leakage	3	1	3	none?	OCV ↓ T ↑ air humidity, λ-sensor, $\Delta P_{an\text{-}cath}$, P2, R_Ω, P5, P3	**C**
	Conductivity loss	1.25	2	2.5	none	R_W	**C**

Process	Attribution	Frequency peak	Influenced by
P1	probably O_2 dissociation	< 1 Hz	j, T
P2	gas conversion	few Hz	j, T, pH_2O, dilution
P3	cathode R_{pol}	10-100 Hz	j, T, pO_2
P4	likely anode diffusion	100-500 Hz	j, T, pH_2O, dilution
P5	anode R_{pol} (ct)	1-4 kHz	j, T, pH_2O, dilution
P6	ion transfer at cathode side	> 5 kHz	T, pO2
R_Ω	anything ohmic	intercept (corrected)	T

9. Summary and Conclusion

Based on this overview, a final ranking is now be specified. The following reordering of the previous table is proposed below:

Component	Process	Risk	Recovery	Detection	Σ
Anode	Reoxidation	4.5	lower UF, **OCV operation; current treatment**	**P5 ;** (P2, R_Ω)	**A**
Anode	C deposition	4.5	**steam/CO_2 flush**, j ↑ (electrochemical oxidation), increase H_2	**Δp(anode, reformer) reformer-T λ-sensors (O/C-ratio) ;** R_Ω ↓ (P2, P5)	**A**
Sealing	Leakage	4.5	**compression** ↑? **self-healing** by T ↑?	**OCV** ↓;T ↑ **cathode outlet humidity** λ-sensor **$\Delta P_{an\text{-}cath}$**, ΔP_{an}, ΔP_{cath}	**A**
MIC	Contact loss	4.5	compression? T ↑?	R_Ω, (P2), Δp cathode?	**B**
MIC	Corrosion + poisoning	4.38	Cr revolatilisation? (OCV or reverse polarity?)	R_Ω (scale); P3 (Cr poisoning); P2 (cathode pore blocking)	**B/C**
Anode	S poisoning	3.94	stop S-flow; T ↑ H_2-operation	S-detector at trap outlet; P5,P2	**B**
Cathode	Demixing	3.75	T_{op} ↑ ?; η_{cath} ↑ or η_{an} ↑? (controversial); operation at **reduced pO_2 (e.g. 5%)?**	**P3** (R_{pol}), **P1** (O_2-dissoc), (R_Ω), P2 (when reduced porosity)	**B**
Sealing	Reactivity + Poisoning	3.38	self-healing by T ↑?	OCV ↓T ↑air humidity, λ-sensor, $\Delta P_{an\text{-}cath}$, ΔP_{an}, ΔP_{cath}, P3/P5 (poisoning), P2	**B/C**
Anode	Coarsening	3	Current treatment	P5, P2, R_Ω	**C**
Electrolyte	Leakage	3	none?	OCV ↓T ↑air humidity, λ-sensor $\Delta P_{an\text{-}cath}$, P2, R_Ω, P5, P3	**C**
Cathode	$SrZrO_3$ formation	2.81	none	R_Ω ?, P3?	**C**
Electrolyte	Conductivity loss	2.5	none	R_W	**C**

INSIGHT would thus suggest to consider the top 3 rows for detailed investigation and application of detection and mitigation measures in the project :

1. **Anode reoxidation**. **Detection** on the **P5** anode charge transfer signal (increase) occuring around **1 kHz**, and **recovery** study by **current treatment**.

2. **Carbon deposition**. **Detection** by **pressure drop increase** (reformer, stack anode), potentially on the **P2** gas conversion process (increase) around a **few Hz** and a temporary decrease in series resistance **R_Ω**; **recovery** study by a change in **anode gas composition** (steam / CO_2 flush, higher H_2) and **increase of operating current** to electrochemically reoxidize deposited carbon.

3. **Sealing leakage**. **Detection** by an increase in **cathode outlet humidity** and a **decrease in pressure drops** (cathode, anode, cathode vs anode, depending on where leakage may occur), and **recovery** study by temporary **temperature increase and compression increase combined with reduced gas flows** to explore self-healing of the leak(s).